Monthly Notices
of the
ROYAL ASTRONOMICAL SOCIETY

MNRAS **435,** 1198–1232 (2013) doi:10.1093/mnras/stt1365
Advance Access publication 2013 August 26

Metals in the IGM approaching the re-ionization epoch: results from X-shooter at the VLT*

V. D'Odorico,[1]† G. Cupani,[1] S. Cristiani,[1,2] R. Maiolino,[3,4,5] P. Molaro,[1] M. Nonino,[1] M. Centurión,[1] A. Cimatti,[6] S. di Serego Alighieri,[7] F. Fiore,[3] A. Fontana,[3] S. Gallerani,[8] E. Giallongo,[3] F. Mannucci,[7] A. Marconi,[9] L. Pentericci,[3] M. Viel[1,2] and G. Vladilo[1]

[1]*INAF–OATS, Via Tiepolo 11, I-34143 Trieste, Italy*
[2]*INFN/National Institute of Nuclear Physics, via Valerio 2, I-34127 Trieste, Italy*
[3]*INAF–OAR, via di Frascati 33, I-00040 Monte Porzio Catone, Italy*
[4]*Cavendish Laboratory, University of Cambridge, 19 JJ Thomson Avenue, Cambridge CB3 0HE, UK*
[5]*Kavli Institute for Cosmology, Madingley Road, Cambridge CB3 0HA, UK*
[6]*Dipartimento di Astronomia, Università di Bologna Via Ranzani 1, I-40127 Bologna, Italy*
[7]*INAF–OAArcetri, Largo Enrico Fermi 5, I-50125 Firenze, Italy*
[8]*Scuola Normale Superiore di Pisa, Piazza dei Cavalieri 7, I-56126 Pisa, Italy*
[9]*Dipartimento di Fisica e Astronomia, Università di Firenze, via G. Sansone 1, I-50019 Sesto Fiorentino, Firenze, Italy*

Accepted 2013 July 22. Received 2013 June 18; in original form 2012 October 16

ABSTRACT

We present the results of observations taken with the X-shooter spectrograph devoted to the study of quasars at $z \sim 6$. This paper focuses on the properties of metals at high redshift traced, in particular, by the C IV doublet absorption systems. Six objects were observed with resolutions $\simeq$27 and 34 km s^{-1} in the visual, and 37.5 and 53.5 km s^{-1} in the near-infrared. We detected 102 C IV lines in the range: $4.35 < z < 6.2$ of which 27 are above $z \sim 5$. Thanks to the characteristics of resolution and spectral coverage of X-shooter, we could also detect 25 Si IV doublets associated with the C IV at $z \gtrsim 5$. The column density distribution function of the C IV line sample is observed to evolve in redshift for $z \gtrsim 5.3$, with respect to the normalization defined by low-redshift ($1.5 < z < 4$) C IV lines. This behaviour is reflected in the redshift evolution of the C IV cosmic mass density, $\Omega_{\rm C\,IV}$, of lines with column density in the range $13.4 < \log N({\rm C\,IV}) < 15$, which is consistent with a drop of a factor of $\sim$2 for $z \gtrsim 5.3$. Considering only the stronger C IV lines ($13.8 < \log N({\rm C\,IV}) < 15$), $\Omega_{\rm C\,IV}$ gently rises by a factor of $\sim$10 between $z \simeq 6.2$ and $z \simeq 1.5$ with a possible flattening towards $z \sim 0$. The increase is well fitted by a power law: $\Omega_{\rm C\,IV} = (2 \pm 1) \times 10^{-8}[(1+z)/4]^{-3.1\pm0.1}$. An insight into the properties of the C IV absorbers and their evolution with redshift is obtained by comparing the observed column densities of associated C IV, Si IV and C II absorptions with the output of a set of CLOUDY photoionization models. As already claimed by cosmological simulations, we find that C IV is a good tracer of the metallicity in the low-density intergalactic medium (IGM) gas at $z \sim 5-6$ while at $z \sim 3$ it arises in gas with overdensity $\delta \sim 100$.

Key words: galaxies: abundances – intergalactic medium – quasars: absorption lines – cosmology: observations.

1 INTRODUCTION

The properties of stars, galaxies and quasars in the local and early Universe can be investigated through their impact on the intergalactic medium (IGM). In particular, the radiation emitted and the metals ejected from these objects re-ionized and polluted the IGM. As a consequence, the detailed understanding of these mechanisms has the potential to significantly constrain models for the formation and evolution of galaxies and quasars, and the re-ionization history of

*Based on observations collected at the European Southern Observatory Very Large Telescope, Cerro Paranal, Chile – Programmes 069.A-0529, 079.A-0226, 084.A-0390, 084.A-0550, 085.A-0299, 086.A-0162, 087.A-0607 and 268.A-5767.

† E-mail: dodorico@oats.inaf.it

the Universe. The IGM is mainly studied through the absorption signature it leaves in the spectra of bright high-redshift sources, quasars and gamma-ray bursts. The highest redshift quasars have been detected mainly by the Sloan Digital Sky Survey (SDSS) at $z \sim 6$ (e.g. Fan et al. 2001), corresponding to ∼1 billion years after the big bang. This sample of ∼20 objects has been used to investigate several topics, in particular the ionization and chemical status of the IGM at these high redshifts (see Fan, Carilli & Keating 2006 for a review).

The same high-z quasars can be used to put an indirect constraint on the epoch of re-ionization by investigating the redshift evolution of metal abundances traced by ionic absorption lines. The investigation of the regime beyond $z \sim 5$ is essential since in this redshift range the comoving star formation rate density appears to decline with redshift (e.g. Mannucci et al. 2007; Gonzàlez et al. 2010). If a similar behaviour is observed for the mass density of metals in the IGM, then a scenario where winds from in situ star-forming galaxies pollute the IGM with metals would be favoured. On the other hand, if the mass density of metals is observed to remain constant, this would point to an epoch of very early enrichment of the IGM, presumably by massive stars (e.g. Pop III stars) in mini-haloes ($M \sim 10^6\,\mathrm{M}_\odot$; e.g. Choudhury, Ferrara & Gallerani 2008), when shallow potential wells allow winds to distribute metals over large comoving volumes, thus producing a quite uniform metallicity distribution (e.g. Madau, Ferrara & Rees 2001). These same massive stars could have been the main sources of ionizing photons allowing for an earlier re-ionization epoch.

Recent estimates of the evolution with redshift of the C IV cosmic mass density (see definition in Section 5.2; D'Odorico et al. 2010; Cooksey et al. 2013) show a decrease of the C IV content from redshift ∼0 to 3, and then a flat behaviour in the range $z \simeq 3$–5 and a possible downturn at $z > 5$. Searching for intergalactic C IV absorption lines at $z > 5$ becomes challenging because the C IV doublet moves into the near-infrared spectral region; absorption line spectroscopy is much more difficult in this regime because of increased detector noise, OH emission from the sky and more severe telluric absorption.

The first results at $z \gtrsim 5.5$ were based on low/intermediate-resolution QSO spectra and a few detections of C IV absorptions indicating a possible decrease of the value of $\Omega_{\mathrm{C\,IV}}$ (Ryan-Weber et al. 2009) and a significant decline of the C IV column density distribution function (CDDF; Becker, Rauch & Sargent 2009). In a recent work, Simcoe et al. (2011, hereafter Simcoe11) claim the presence of a downturn in the C IV abundance at $\langle z \rangle = 5.66$ by a factor of 4.1 relative to its value at $\langle z \rangle = 4.96$. The result is based on the spectra (at resolution $\delta v \simeq 50\,\mathrm{km\,s^{-1}}$) of seven quasars obtained with the new spectrograph FIRE (Simcoe et al. 2010) at the Magellan telescope, coupled with six observations of northern objects taken from the literature, of which four (see Ryan-Weber et al. 2009) have three times lower resolution and lower signal-to-noise ratio than the FIRE sample. The northern sample shows only one C IV absorption system, while almost doubling the surveyed redshift path, the effect is a decrease of the value of $\Omega_{\mathrm{C\,IV}}$, which however could be due to the lower quality of those spectra.

In this work, we present the spectra obtained in a Guaranteed Timed Observation (GTO) programme (PI: V. D'Odorico) carried out with the X-shooter spectrograph at the European Southern Observatory (ESO) Very Large Telescope (VLT) between 2010 January and 2011 June. The scientific aim of this project was to observe the brightest ($J_{\mathrm{Vega}} \lesssim 19$) quasars known with $z_{\mathrm{em}} \gtrsim 5.7$ and observable from Paranal to derive constraints both on the abundance of neutral hydrogen and on the abundance of metals at high redshift. Here the results on the metal lines are reported; the H I abundance will be the topic of a forthcoming paper. The X-shooter spectrograph (Vernet et al. 2011), with its high sensitivity, extended spectral coverage (from 3000 Å to 2.5 μm) and intermediate resolution, appeared to be the ideal instrument to allow significant steps forward in this research field. Seven objects satisfy the chosen selection criteria. However, only four of them were observed due to bad weather downtime. Luckily, two of the objects we could not observe are present in the ESO X-shooter archive and we have retrieved and analysed their spectra.

Preliminary results on a sample of three objects (J1306+0356, J0818+1722, J1509−1749) were reported in D'Odorico et al. (2011, hereafter Paper I). Here, we describe the whole sample and carry out a more detailed analysis.

The rest of the paper is organized as follows. Data reduction and analysis are presented in Section 2. In Section 3, the spectra of each object in the sample are described in detail. Section 4 is dedicated to the C IV lines statistics: CDDF and cosmic mass density. The results are discussed in Section 6. Throughout this paper, we assume $\Omega_{\mathrm{m}} = 0.26$, $\Omega_\Lambda = 0.74$ and $h \equiv H_0/(100\,\mathrm{km\,s^{-1}\,Mpc^{-1}}) = 0.72$.

2 OBSERVATIONS AND DATA REDUCTION

The spectra were acquired with a binning of two pixels in the dispersion direction and adopting two sets of slit apertures for the blue, visual (VIS) and near-infrared (NIR) arms, respectively: 1.0/0.9/0.9 and 0.8/0.7/0.6 arcsec depending on the seeing conditions at the moment of the observations. The journal of observations is reported in Table 1.

All the raw frames were reduced with the public release of the X-shooter pipeline (Goldoni et al 2006). The pipeline reduction proceeds along the following steps. Pixels in the 2D frames are first mapped to wavelength space using calibration frames. Sky emission lines are subtracted before any re-sampling using the method

Table 1. X-shooter observations. Spectra of J0818+1722, J1509−1749 and J1030+0524 were obtained using the combination of slits 1.0/0.9/0.9 arcsec in the UVB/VIS/NIR arms, while for the frames of J0836+0054, J1306+0356 and J1319+0950, the combination 0.8/0.7/0.6 arcsec was adopted. ΔX is the redshift absorption path defined in Section 5.1 and the SNR is computed per resolution element.

QSO	z_{em}	J_{mag}	T_{VIS} (s)	T_{NIR} (s)	SNR @ (9000 Å)	SNR @ (10 350 Å)	$z_{\mathrm{C\,IV}}$	$\Delta X_{\mathrm{C\,IV}}$	$z_{\mathrm{Si\,IV}}$
J0818+1722[a]	6.002	18.54	22 910	23 390	85	24	4.516−5.886	6.646	5.128−5.886
J0836+0054[b]	5.810	17.9	8160	8400	65	10	4.365−5.697	6.371	4.960−5.697
J1030+0524[b]	6.308	18.87	26 860	26 000	125	7	4.757−6.187	7.091	5.395−6.187
J1306+0356[b]	6.016	18.77	46 800	46 800	55	12	4.527−5.900	6.666	5.140−5.900
J1319+0950[c]	6.13	18.8	36 000	36 000	95	15	4.617−6.012	6.831	5.240−6.012
J1509−1749[d]	6.118	18.78	23 360	24 000	50	8	4.608−6.000	6.814	5.229−6.000

[a]Fan et al. (2006); [b]Fan et al. (2001); [c]Mortlock et al. (2009); [d]Willott et al (2007).

developed by Kelson (2003). The different orders of the echelle spectrum are then extracted, rectified, wavelength calibrated and merged, with a weighted average used in the overlapping regions. The final product is a 1D, background-subtracted spectrum and the corresponding error file. The spectra are re-binned to 0.3 (narrow slit) or 0.4 Å (broad slit) in the VIS and to 0.6 Å in the NIR arm, following the prescription of the pipeline manual.

We followed the standard procedure with the exception of the extraction of the 1D spectrum from the 2D merged spectrum which was carried out with the EXTRACT/LONG command in MIDAS reduction package (using a predefined aperture). The extraction within MIDAS results in a better signal-to-noise ratio at least for those objects which are faint and whose spectrum is strongly absorbed in the Lyα forest region. The instrument response curve was obtained reducing with the specific pipeline recipe the standard flux stars observed the same night of the scientific observations. Each extracted frame was then flux calibrated by dividing for the response curve. Finally, the set of 1D spectra obtained for each object was added with a weighted sum to obtain the final spectrum.

The continuum level in the region redwards of the Lyα emission was determined interpolating with a spline polynomial of third degree the portions of the spectrum free from absorption lines. The same approach cannot be applied to the heavily absorbed Lyα forest. The continuum in this spectral range was obtained by extrapolating the power law which fits the red region cleaned from the intrinsic emission lines.

Finally, the VIS and NIR spectra were corrected for telluric absorption dividing by the normalized spectrum of standard spectroscopic stars observed with the same instrumental set-up as the quasars in our sample, using the command *telluric* in IRAF.

2.1 Identification of metal absorptions

Metal absorptions redwards of the Lyα emission have been identified mainly by eye. First, we looked for the most common ion doublets and multiplets (e.g. C IV, Mg II, Fe II and Si IV) and fitted them to confirm their nature and determine a precise redshift. Then, the lines without an identification were processed with automatic routines which try to associate those lines with the identified systems or with known ions on the basis of their wavelength ratios.

In the VIS region of the spectrum, the section inspected for metals extends from the observed wavelength of the Lyα emission to $\lambda = 10\,200$ Å, while in the NIR spectra it goes from this wavelength to $\sim$2 μm, with the known gaps due to atmospheric absorption. At $\lambda > 2$ μm, telluric lines are severely affecting the spectrum preventing the detection of other absorption lines. The redshift range of the C IV and Si IV forests reported in Table 1 goes from the Lyα emission $+1000\,\mathrm{km\,s^{-1}}$, to avoid blending with Lyα lines, to the C IV and Si IV emission, respectively, $-5000\,\mathrm{km\,s^{-1}}$, to avoid proximity effects.

The analysis of high-resolution spectra (full width at half-maximum $\simeq$6–7 $\mathrm{km\,s^{-1}}$) shows that metal lines are characterized by Doppler velocity widths of the order of 5–10 $\mathrm{km\,s^{-1}}$ (e.g. Tescari et al. 2011), which are not resolved in the X-shooter spectra. In spite of this, we have fitted the detected metal lines (in particular, C IV and Si IV) with Voigt profiles using the context LYMAN of the MIDAS reduction package (Fontana & Ballester 1995). None of the fitted doublets shows saturation (the strength ratio in the doublet would not be preserved in that case), so we are confident that we are not underestimating their true column densities.

For comparison with previous works, we have also computed the rest-frame equivalent widths, W_0, of C IV and Si IV doublets by direct summation of the continuum-normalized flux of the spectral pixels. The errors on W_0 were computed as the square root of the quadratic sum of the flux standard deviations. The sums have been performed over the velocity range extending between the two pixels at which the normalized profile returned to unity. In the case of blending with other transitions, we report either a lower or an upper limit to the equivalent width depending on whether only part of the line profile is blended with a nearby absorption or the considered line falls within other strong absorptions (e.g. telluric line). In the case of complex velocity profiles if components are blended, we measured the total equivalent width. Tables A1–A6 report the equivalent width and the measured column density of all the C IV and Si IV lines detected in our spectra.

The level of completeness of our sample was computed by generating a set of mock C IV absorption doublets with column densities in the range 13.3–13.8 and random redshifts in the interval covered by the observed spectra. Doppler parameters were derived randomly from a list of measured Doppler parameters for the X-shooter observed C IV sample. The correct velocity profiles for the lines were obtained with the procedure COMPUTE/LYMAN in MIDAS, and the lines were then superposed to the observed spectra and detected by eye. Our X-shooter spectra result to be complete to almost 100 per cent for C IV doublets with $\log N(\mathrm{C\,IV}) \geq 13.6$ for the whole inspected redshift range. Considering the redshift range $z < 5.3$, the sample is complete to above 95 per cent for $\log N(\mathrm{C\,IV}) = 13.5$ and 13.4, and at 85 per cent for $\log N(\mathrm{C\,IV}) = 13.3$. Above $z = 5.3$, the completeness decreases significantly with C IV lines with column density in log equal to 13.5 detected 85 per cent of the time, 13.4 detected 70 per cent of the time and 13.3 in 60 per cent of the cases.

3 NOTES ON INDIVIDUAL OBJECTS

In this section, all the objects in the sample are briefly introduced. We report also on the objects already described in Paper I, since some variations occurred with the improvement of the reduction pipeline and the optimization of our procedure.

In the following, all the reported signal-to-noise ratios (SNR) are per resolution element. The resolution in the VIS arm is $R \simeq 8800$ and 11 000 for the 0.9 and 0.7 arcsec slits, respectively; while in the NIR arm it is $R \simeq 5600$ and 8000 for the 0.9 and 0.6 arcsec slits. The redshift of absorption systems is reported with the number of significant digits (in general four or five); in the case of systems with a complex velocity structure, the average redshift is reported with three decimal digits.

3.1 SDSS J0818+1722

This object, which has the best SNR in our sample, was already discussed in Paper I.

The VIS portion of the spectrum outside the Lyα forest is the richest in absorption lines; having a large SNR (=120–60) we could subtract quite well the telluric features revealing the presence of many absorption systems. In the NIR portion of the spectrum, the SNR lower to $\sim$10–15 in the z band, to increase again to $\sim$50–100 in the J and H bands.

We detected C IV doublets at $z_{\mathrm{abs}} = 4.462\,98$, 4.498 00, 4.508 38, 4.523 05, 4.620 25, 4.627 02, 4.7263 (complex, detected also by Simcoe11), 4.731 58, 4.877 39 and 4.9417, together with marginal detections (below our 3σ limit) at $z_{\mathrm{abs}} = 4.552\,25$, 4.577 33. Those absorption systems are shown in Figs 1 and 2. The λ 1548 Å C IV line

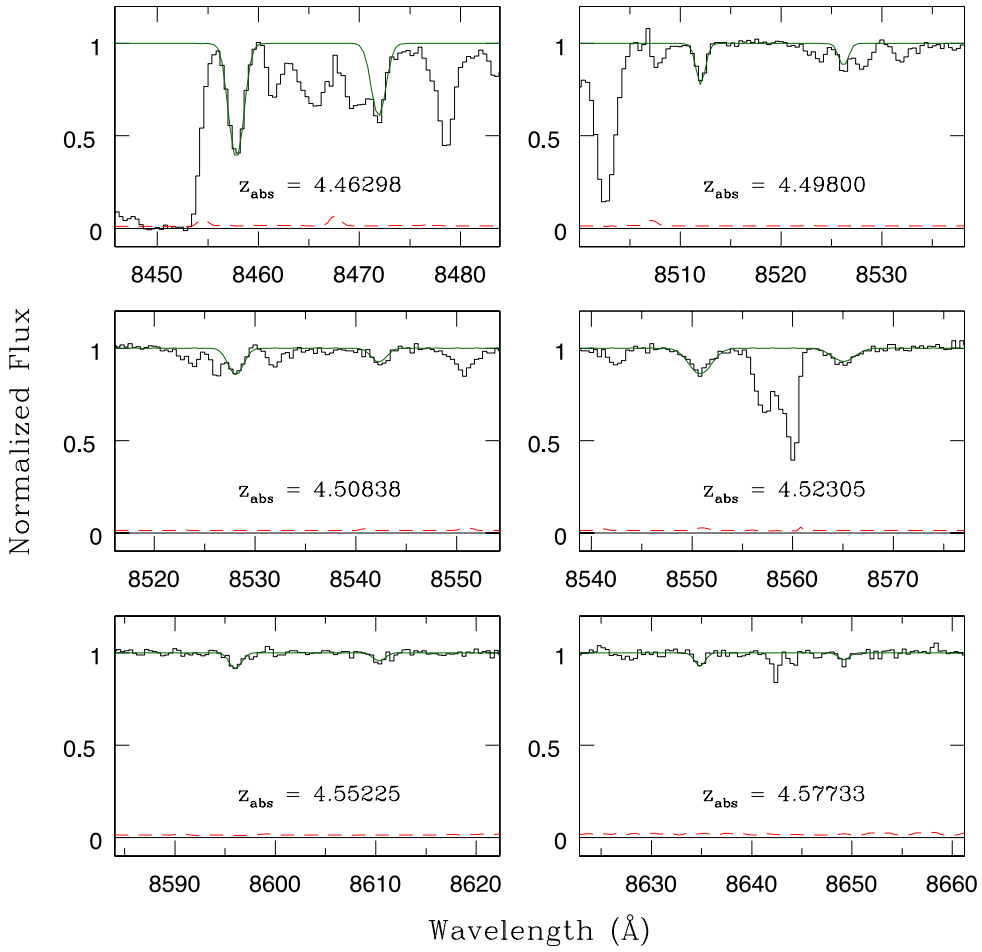

Figure 1. Detected C IV absorption systems in the spectrum of SDSS J0818+1722. The solid histogram shows the observed spectrum, the continuous green line shows the result of the profile fitting while the dashed red line denotes the standard deviation of the flux.

at $z_{\rm abs} = 4.691\,48$, reported in Simcoe11, was identified as the Si IV 1393 Å transition associated with the C IV system at $z_{\rm abs} = 5.322\,26$ (see below).

At $z > 5$, possible C IV doublets with associated Si IV lines were detected at $z_{\rm abs} = 5.064\,67, 5.076\,30, 5.082\,38, 5.322\,26$ and 5.8441, with a marginal detection without Si IV at $z_{\rm abs} = 5.308\,48$. Those C IV systems are shown in Figs 3 and 4.

The spectrum of J0818+1722 is characterized by the presence of the only systems at low ionization above $z \sim 5$ detected in our sample, at $z_{\rm abs} = 5.064\,59$, 5.791 and 5.876 44. For the system at $z_{\rm abs} = 5.064\,59$ (see Fig. 3), it was possible to put an upper limit to the column density of Zn II $\log N({\rm Zn\,II}) \lesssim 12.5$, implying a ratio [Zn/Fe] $\lesssim 1.85$. The latter two systems show also absorption due to O I (see Figs 5 and 6 for all the detected transitions); they were discussed in the work by Becker et al. (2011). The presence of the C IV doublet associated with the system at $z_{\rm abs} = 5.791$ was reported by Ryan-Weber et al. (2009); however, both lines fall on sky lines (see Fig. 5) and in our spectrum they are below $3\,\sigma$ detection. Also the C IV at $z_{\rm abs} = 5.876\,44$ is very uncertain (see Fig. 6).

Two weak Mg II systems were identified at $z_{\rm abs} = 2.090\,59$ and $2.129\,39$; a strong Mg II doublet with associated Fe II 2344, 2382, 2586, 2600 Å absorptions was detected at $z_{\rm abs} = 3.562\,85$. We do not confirm the Mg II system at $z_{\rm abs} = 2.834$ reported by Ryan-Weber et al. (2009). The plots for these systems are shown in Fig. B1 (Appendix B).

3.2 SDSS J0836+0054

This quasar, discovered in the SDSS (Fan et al. 2001), has the lowest redshift, $z_{\rm em} = 5.810$, and is the brightest of the sample.

In the past, it was studied with the Keck both at low and high resolution with ESI, HIRES and NIRSPEC (Pettini et al. 2003; Becker et al. 2006, 2009), with GNIRS@Gemini (Jiang et al. 2007) and with ISAAC@VLT (Ryan-Weber et al. 2009). Due to very good seeing conditions during the observations, we could observe this object at a higher resolution than the others in the sample: $R \simeq 11\,000$ and 8000 in the VIS and NIR arms, respectively. The X-shooter spectrum has an SNR $\sim 90-50$ in the range $\lambda\lambda\,8300-9300$ Å, decreasing to $8-20$ in the z band and increasing again to SNR $\sim 30-37$ in the J and H bands.

We identify a previously unknown Mg II system at $z_{\rm abs} = 2.2990$ with associated Fe II 2600 and 2586 Å, and we confirm the Mg II system reported by Jiang et al. (2007) at $z_{\rm abs} = 3.7435$ detecting also the associated Al III doublet and Fe II 2600 and 2382 Å features. Those absorption systems are plotted in Fig. B2 (Appendix B).

As for the C IV doublets, a new entry with respect to Pettini et al. (2003, from now on Pettini03) is found at $z_{\rm abs} = 4.530\,13$. We also improved the fit of the system at $z_{\rm abs} = 4.684\,27$ and $4.686\,51$ deblending the C IV lines from the Al III doublet at $z_{\rm abs} = 3.745$. More C IV detections are present at $z_{\rm abs} = 4.611\,95$, 4.668 40, 4.698 46 and 4.7733. All those C IV systems are shown in Fig. 7. The system in Pettini03 at $z_{\rm abs} = 4.5144$ is not confirmed in our spectrum; the

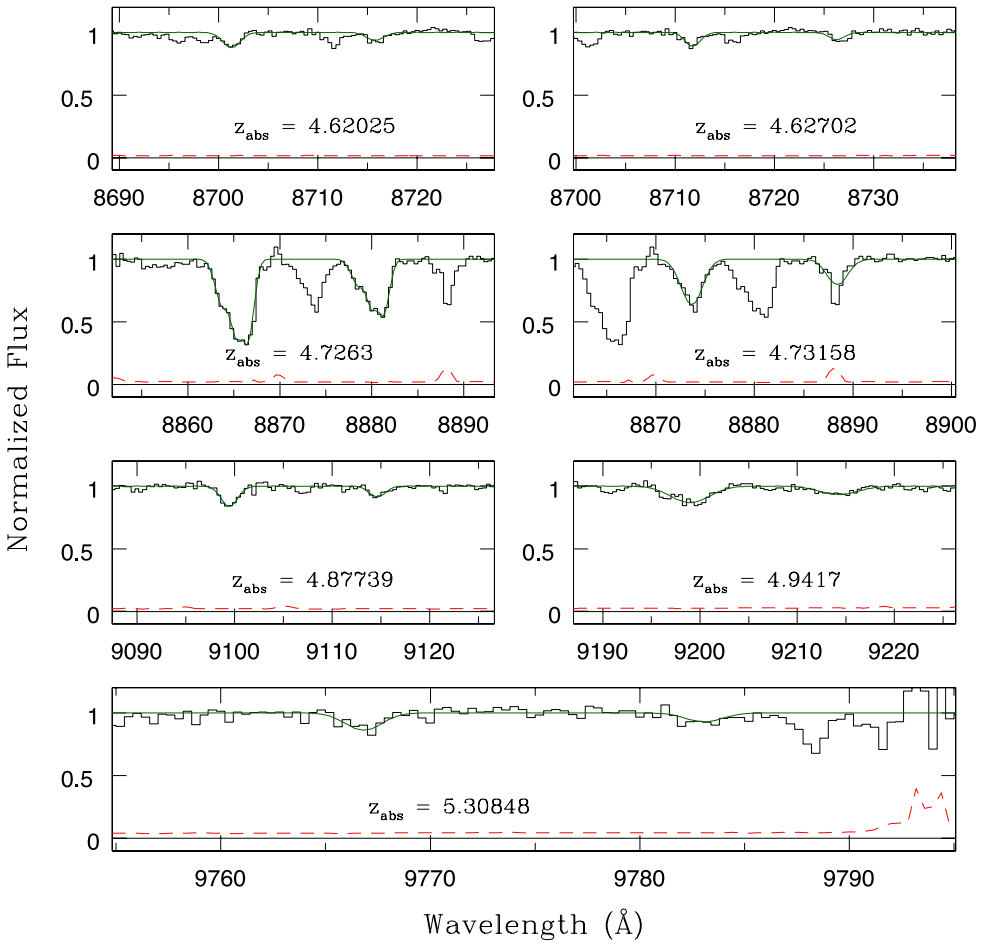

Figure 2. Detected C IV absorption systems in the spectrum of SDSS J0818+1722 (continuation of Fig. 1).

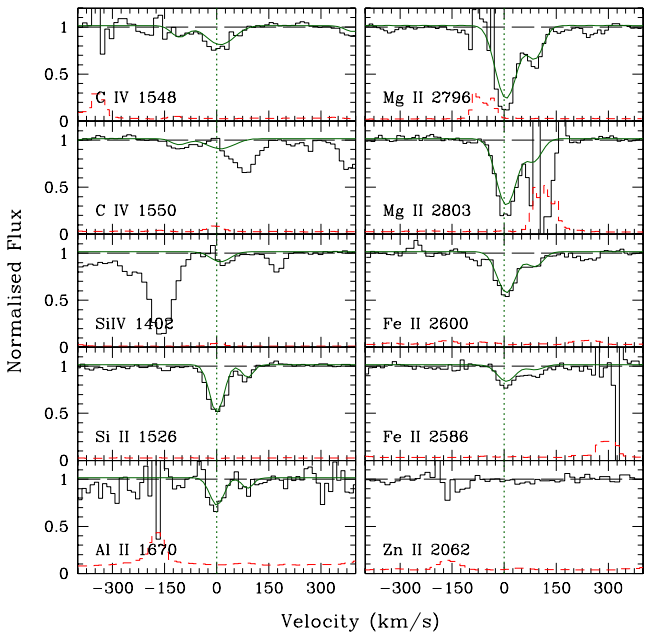

Figure 3. Detected transitions in the absorption system at $z_{\rm abs} = 5.064\,59$ (C IV is at $z_{\rm abs} = 5.064\,67$) in the spectrum of SDSS J0818+1722.

line identified as C IV 1548 Å is in fact Si IV 1393 Å at $z_{\rm abs} = 5.126$ (see below) and the C IV 1550 Å line is probably an artefact of a badly subtracted sky line.

The complex system at $z_{\rm abs} \simeq 4.994$ detected by both Pettini03 and Simcoe11 is confirmed by our data. In our spectrum, we detect also the associated Si IV doublet (see Fig. 8) and a complex velocity structure extending for $\sim$400 km s^{-1}.

In this work, we claim the detection of two new C IV systems at $z > 5$ in the spectrum of J0836+0054 (see Fig. 8). A strong Si IV at $z_{\rm abs} \simeq 5.126$ with two velocity components is observed in the VIS region of the spectrum; unfortunately the associated C IV absorption falls in a region badly contaminated by telluric lines. We partially corrected for them, but the column density resulting from the fit can be considered only as an upper limit. A marginal C IV detection strengthened by the presence of the associated Si IV 1393 Å line is observed at $z_{\rm abs} = 5.322\,77$.

3.3 SDSS J1030+0524

This object has been thoroughly studied in the past being the highest redshift quasar observable from the Southern hemisphere before the recent discovery of the QSO ULAS J1120+0641 at $z = 7.0842$ (Mortlock et al. 2011).

Pettini03, by using spectra obtained with ESI at the Keck telescope, detected a strong C IV system at $z_{\rm abs} = 4.9482$; Ryan-Weber, Pettini & Madau (2006) identified two C IV doublets at $z_{\rm abs} = 5.7238$

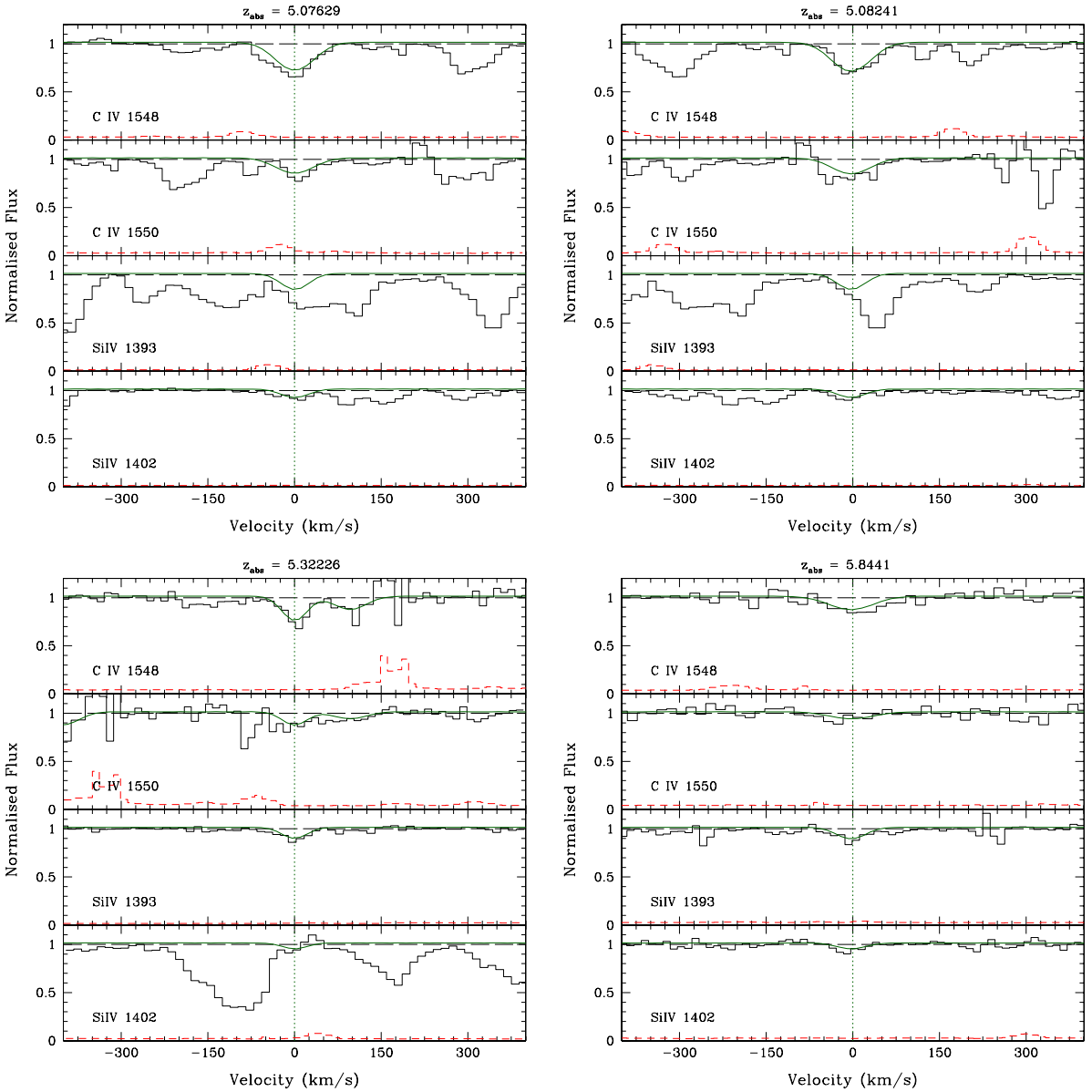

Figure 4. Detected C IV absorption systems with associated Si IV doublets at $z_{\rm abs} > 5$ in the spectrum of SDSS J0818+1722. The strong absorption lines blended with the Si IV doublets at $z_{\rm abs} = 5.076\,30$, 5.082 38 and 5.322 26 are telluric lines that we could not correct.

and 5.829 in the ISAAC spectrum, which are the main contributors to their measurement of $\Omega_{\rm C\,IV}$ (see also Ryan-Weber et al. 2009).

No low-ionization systems were detected at $z > 5$ both in the low (Jiang et al. 2007; Kurk et al. 2007) and high (Becker et al. 2006) resolution spectra of this object.

The X-shooter spectrum has an SNR = 140−50 in the region between the Lyα emission and λ 9300 Å decreasing to ∼10 in the z band and increasing again to ∼20−30 in the J and H bands.

By deblending two complex velocity profiles in the visible region of the spectrum, we identified two possible new C IV doublets at $z_{\rm abs} = 4.766\,71$ (but see Section 4.1) and 4.799 (complex). Another, C IV doublet was identified at $z_{\rm abs} = 4.890\,66$ (but see Section 4.1). We confirm the presence of the C IV system at $z_{\rm abs} = 4.9482$ detected by Pettini03, with which we associate also the Mg II doublet in the NIR region of the spectrum. Si II 1526 and Al II 1670, whose presence is claimed by Simcoe11, are not detected in our spectrum: in particular, the former if present would be blended with the Si IV 1393 at $z_{\rm abs} = 5.5165$. The strong C IV lines at this redshift are clearly detected in our spectrum. This system shows associated low-ionization lines: Al II 1670 and several transitions due to Fe II (λ 2344, 2382, 2586, 2600 Å) in the NIR portion of the spectrum.

The previously identified C IV doublet at $z_{\rm abs} = 5.724\,18$ is present also in our spectrum, but no other associated line has been detected (Si IV is blended with strong telluric lines, but it was detected in the HIRES spectrum by Becker et al. 2009). Recently, Díaz et al. (2011) have claimed the association between this C IV absorption system and a Lyα emitter at $z = 5.719$, lying at a projected distance of 79 physical kpc from the line of sight. This is the highest redshift galaxy–absorber pair detected to date, supporting the idea that galaxy-wide outflows were already in place at the end of the epoch of re-ionization.

A weak C IV doublet (below 3σ) is detected at $z_{\rm abs} = 5.7425$; its nature is confirmed by the presence of the associated transitions due to C II 1334, Si IV 1393 and Fe II 2374, 2382, 2586, 2600 Å.

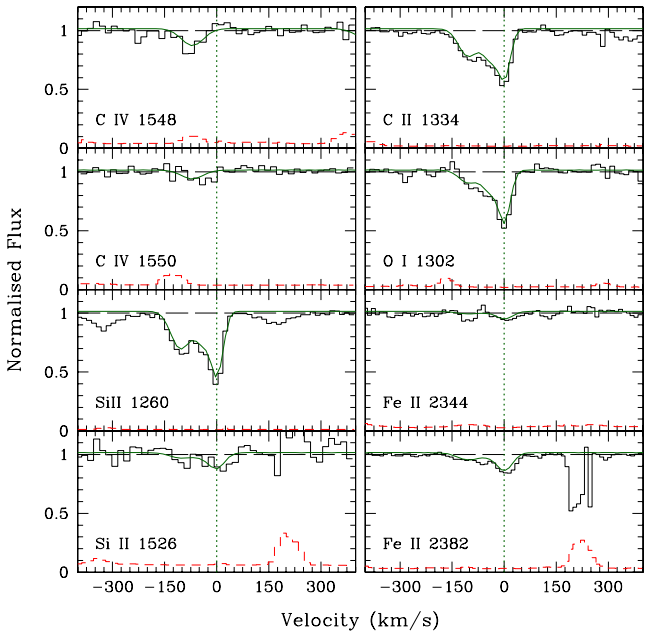

Figure 5. Detected transitions in the absorption system at $z_{abs} = 5.791$ in the spectrum of SDSS J0818+1722.

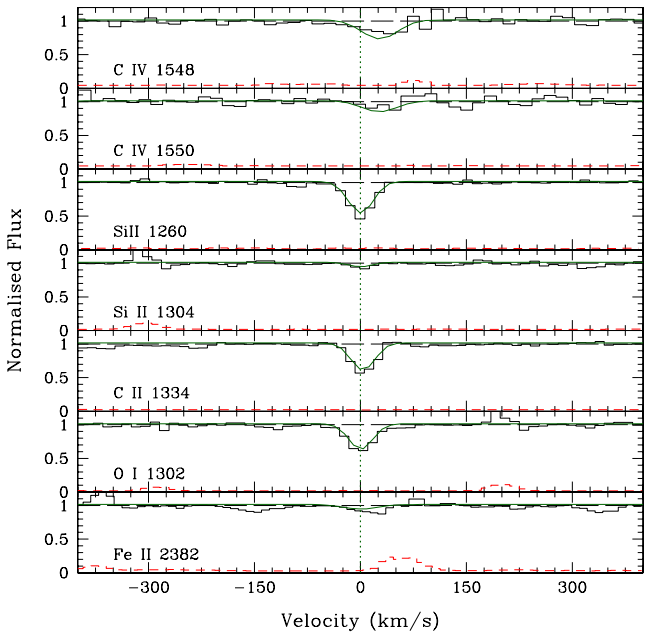

Figure 6. Detected transitions in the absorption system at $z_{abs} = 5.876\,44$ in the spectrum of SDSS J0818+1722.

We tentatively identify a C IV doublet at $z_{abs} = 5.977$ with possible associated Si IV doublet (but slightly shifted in redshift). All the C IV doublets in the spectrum of J1030+0524 are shown in Figs 9 and 10.

The C IV at $z_{abs} = 5.829$ detected by Ryan-Weber et al. (2006) was a misidentification: it is a strong, complex Mg II doublet at $z_{abs} = 2.779$ showing also several associated Fe II transitions (λ 2344, 2382, 2586, 2600 Å). Another strong Mg II doublet is present at $z_{abs} = 4.5836$ with associated Fe II 2344 and 2382 Å lines. A weak Mg II doublet was detected at $z_{abs} = 2.1879$. All Mg II systems are plotted in Figs B3 and B4 (Appendix B).

3.4 SDSS J1306+0356

This object was observed during the commissioning of X-shooter. The VIS portion of the spectrum was discussed in Paper I, while the NIR portion of the spectrum had an SNR too low to be used.

Here we present new observations taken from the ESO VLT archive which improves significantly the SNR of the spectrum. Furthermore, these new observations were obtained with a narrow slit increasing the resolution to $R = 11\,000$ and 8000 in the VIS and NIR arms, respectively. SNR goes from ∼120 to 50 in the region between Lyα emission and 9300 Å, decreasing to ∼10 in the centre of the z band to increase again to ∼25 and 40 in the J and H bands, respectively.

The stronger systems at $z_{abs} = 4.6146$, 4.668, 4.8642 (complex system, extending over more than 600 km s^{-1}) and 4.8808 were confirmed also by Simcoe11. We report new detections at $z_{abs} = 4.528\,97$, 4.653 61, 4.7111, 4.723 15, 4.820 48 (but see Section 4.2), 4.886 94 plus a marginal detection at $z_{abs} = 4.5804$. All the identified C IV systems are shown in Figs 11 and 12.

Three new Mg II systems were identified at $z_{abs} = 2.3781$ (with associated Fe II 2586, 2600 Å lines), 3.4900 and 4.139 83 (with associated Fe II 2344, 2374, 2382, 2586, 2600 Å and Al II lines), and the system at $z_{abs} = 2.5329$ (Jiang et al. 2007; Kurk et al. 2007) is confirmed. Furthermore, we detected the low-ionization lines (Mg II; Fe II 1608, 2344, 2374, 2382, 2586, 2600 Å; Al II and Si II 1526 Å) associated with the strong C IV systems at $z_{abs} = 4.6146$, 4.8642 and 4.8808 (see Fig. B6 in Appendix B).

As in previous observations (Ryan-Weber et al. 2006; Simcoe 2006; Simcoe11), we did not identify any reliable metal system at $z \geq 5$ along the line of sight to J1306+0356.

3.5 ULAS J1319+0950

This QSO at $z_{em} = 6.13$ was the most recently discovered of the sample (Mortlock et al. 2009). We obtained observations from the X-shooter archive at a resolution of $R = 11\,000$ and 8000 in the VIS and NIR arms, respectively. This is the only intermediate-resolution spectrum of this object obtained up to now, together with the FIRE spectrum in Simcoe11.

The SNR varies between ∼95 and 65 from the Lyα emission to 9300 Å, decreasing to ∼15 in the centre of the z band. It increases again to SNR ∼30 and 40 in the J and H bands, respectively.

Four new Mg II systems were detected at $z_{abs} = 2.304$, 2.41 (complex system), 4.216 21 (with Al II and Fe II 2382 Å), 4.568 37 (with Al II and Fe II 2382 Å) and 4.662 (complex, associated with a C IV doublet). All Mg II systems are shown in Fig. B7 (Appendix B).

Several new C IV doublets were detected in the VIS portion of the spectrum where the SNR is maximum: at $z_{abs} = 4.612\,72$, 4.653 17, 4.662 (complex system), 4.703 25 and 4.7169, and also marginal detections at $z_{abs} = 4.6293$ and 4.644 78 (see Fig. 13). Above $z > 5$, we report three detections confirmed by the presence of the associated Si IV doublet: $z_{abs} = 5.2644$, 5.374 88 and 5.5730 (with the possible detection of C II 1334 Å). Those three systems are shown in Fig. 14.

3.6 CFHQS J1509−1749

A preliminary spectrum of this object was already presented in Paper I.

The VIS spectrum has an SNR ∼ 65−30 in the region between the Lyαemission and ∼9600 Å, decreasing to ∼10 in the middle of

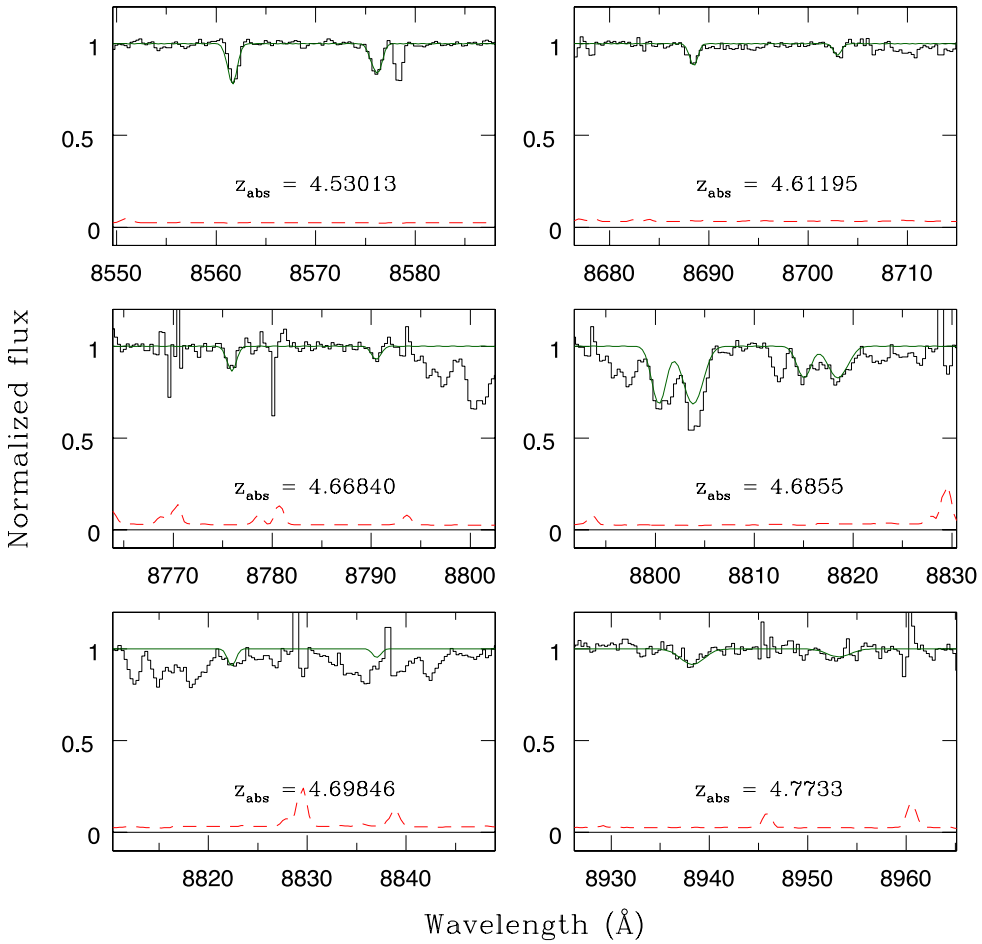

Figure 7. C IV absorption systems detected in the spectrum of SDSS J0836+0054.

the z band. The SNR increases again to ∼20 in the J band and to 25−30 in the H band.

We detected three Mg II systems with associated Fe II 2344, 2382, 2586, 2600 Å transitions at $z_{\rm abs} = 3.1277$, 3.265 74 and 4.0108 (in this case Mg II is blended with telluric lines). The saturated Mg II doublet at $z_{\rm abs} = 3.3915$ presents associated ionic transitions due to Mg I, Mn II, Fe II 2344, 2382, 2600 Å and Zn II 2026 and 2062 Å. The plots of these absorption systems are shown in Fig. B8 (Appendix B).

Eight C IV doublets have been identified at $z_{\rm abs} = 4.610\,86$, 4.641 88, 4.6501, 4.655 08, 4.666 29, 4.7690, 4.791 82 and 4.815 68. All C IV doublets are shown in Fig. 15.

We propose also an alternative identification for the C IV doublets at $z_{\rm abs} = 4.641\,88$, 4.6501 and 4.666 29. After the identification of a weak Al III doublet at $z_{\rm abs} = 3.7205$, we realized that the lines identified as C IV could also be part of a complex Al III system at $z_{\rm abs} \sim 3.716$, where the first two velocity components happen to have the separation and the column density ratio of a C IV doublet. The system is plotted in Fig. 16. The absence of Fe II transitions could be an argument in favour of the C IV nature of the lines; however, there are no other pieces of strong evidence to make us prefer one or the other identification. This alternative identification of the three C IV doublets does not affect the computation of $\Omega_{\rm C\,IV}$ since the lines all have $\log N({\rm C\,IV}) < 13.4$.

At $z > 5$, the presence of the C IV system at $z_{\rm abs} = 5.915\,72$ claimed by Simcoe11 is confirmed in our NIR spectrum and is reinforced by the detection of the associated Si IV doublet. The system is shown in Fig. 17.

4 UVES SPECTRA

In this section, we briefly report on the analysis of the high-resolution spectra of SDSS J1030+0524, SDSS J1306+0356 and SDSS J1044−0125 obtained with the UV and Visual Echelle Spectrograph (UVES; Dekker et al. 2000) at the ESO VLT telescope. They were all observed by our group but the data have not been published before. The journal of observations is reported in Table 2.

The individual spectra were reduced and wavelength calibrated by using the UVES pipeline (Ballester et al. 2000). Wavelengths were then corrected to the vacuum heliocentric reference system. Fast rotator stars observed the same nights as the QSO were also reduced in order to identify telluric absorptions in QSO spectra. The final spectrum is computed as a weighted mean of the single frames. The SNR is in general quite low for all spectra; however, the higher resolution allowed us to exclude the presence of some of the weakest systems detected in the X-shooter spectra.

4.1 SDSS J1030+0524

We used all the seven spectra existing in the UVES archive, obtained in six consecutive nights at the end of April and beginning of 2002

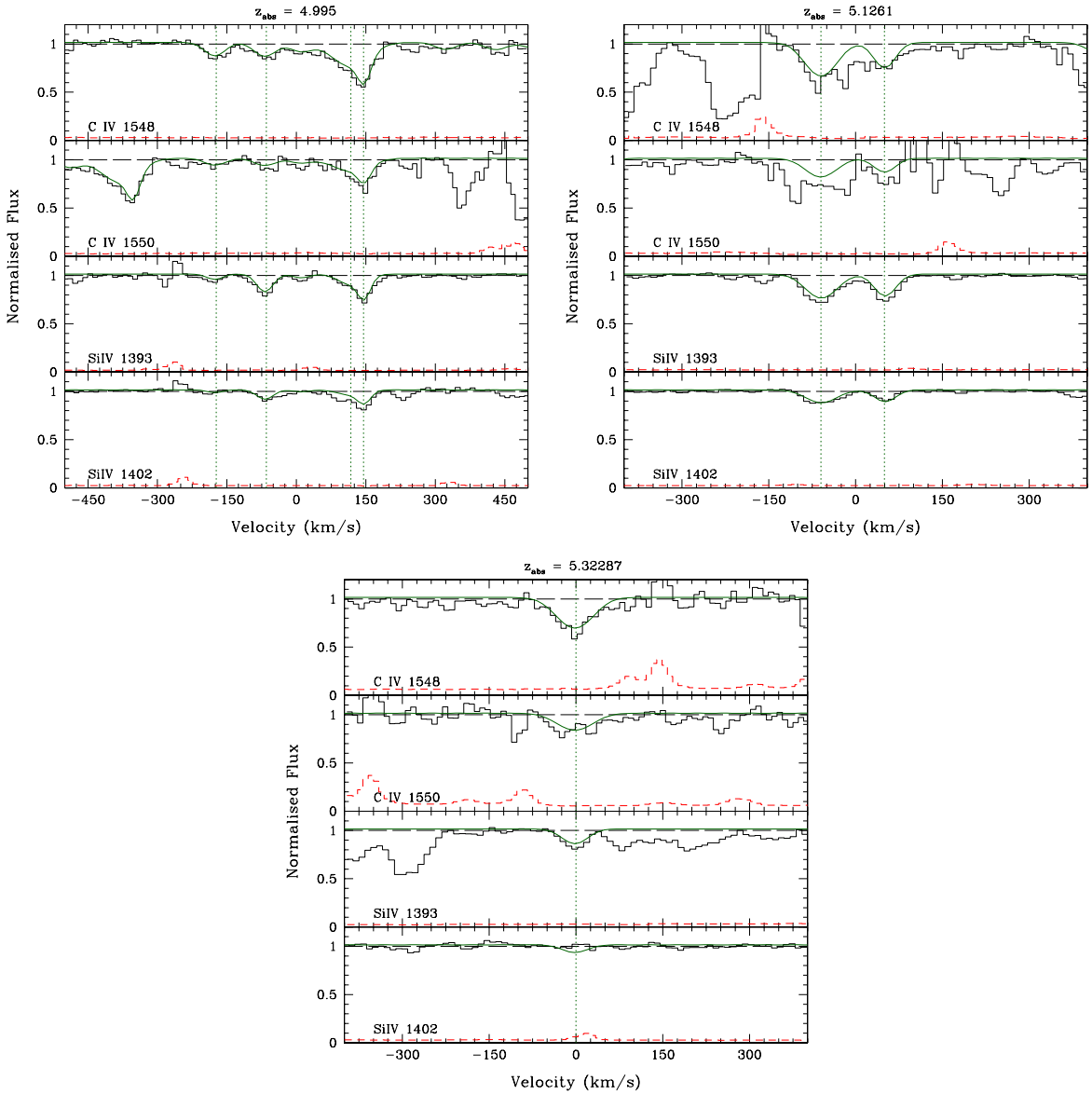

Figure 8. C IV absorption systems with associated Si IV doublets in the spectrum of SDSS J0836+0054.

May. Only the red arm was used for these observations at central wavelengths λλ7940 and 8140 Å, with slit width of 1 arcsec and binning of 2×2.

We looked for metals in the region 8760 < λ < 9900 Å, outside the Lyα forest and common to the two settings. The SNR varies from 20 to 5 in the reddest part of the spectrum.

Inspection of the high-resolution spectrum of J1030+0524 did not confirm the presence of two systems detected in the X-shooter spectrum: the C IV doublets at $z_{\rm abs} = 4.766\,71$ and 4.890 66.

4.2 SDSS J1306+0356

We used two sets of UVES spectra available in the archive, obtained in 2002 and 2007. All the spectra were recorded with binning of 2×2 and slit width of 1 arcsec. Six spectra are from 2002 with a total exposure time of 8.6 h and central wavelengths λλ7940, 8140, 8260, 8040 Å. 10 spectra are from 2007 with a total exposure time of 7.9 h recorded at central wavelength λ8600 Å. In the final spectrum, the region outside the Lyα forest ranges between 8430 and 10 000 Å. For the analysis, we used the average spectra of both sets of data for λ < 9550 Å, with SNR varying from ∼24 to 10 in the interval λλ8725–9550 Å, respectively. For λ > 9550 Å, only the average of the 2002 observations was used with SNR varying between 8 and 5 for the reddest wavelengths, because the spectra taken in 2007 have very poor quality with SNR ∼ 2.

The presence of the C IV doublet at $z_{\rm abs} = 4.820\,48$, detected in the X-shooter spectrum, was not confirmed in this spectrum.

4.3 SDSS J1044−0125

This quasar was excluded from the sample collected with the X-shooter spectrograph because it is a Broad Absorption Line (BAL) object.

In the UVES archive, there are six spectra obtained in March and April of 2002 with the red arm at central wavelength λ8600 Å, with slit width of 1 arcsec and binning of 2×2.

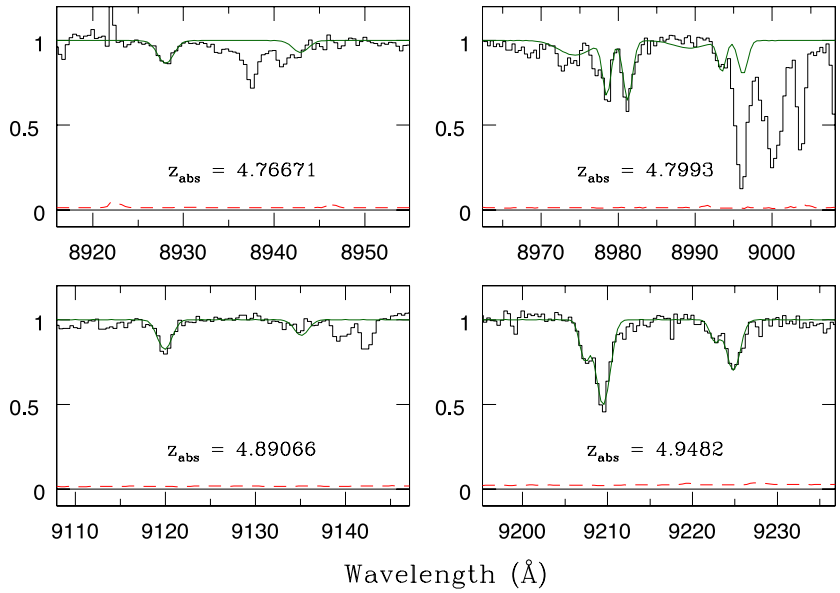

Figure 9. Detected C IV absorption systems in the spectrum of SDSS J1030+0524.

The final spectrum covers the ranges λλ6710−8520 and 8669−9855 Å, even though the flux is not zero at $\lambda > 8150$ Å. The quality of the final spectrum is quite poor with an SNR of the order of 10.

A single feature is observed which was identified as C II 1334 Å at $z_{\rm abs} \simeq 5.2847$. No other associated transitions were detected in the UVES spectrum.

Songaila & Cowie (2002) claimed the detection of the Fe II 1608 Å line at the same redshift in the ESI spectrum and derived an estimate of the metallicity of [Fe/H] = −2.65. On the other hand, no absorption lines were detected in the higher resolution spectrum obtained with MIKE@Keck by Becker et al. (2011).

5 C IV LINE STATISTICS

5.1 The C IV CDDF

The CDDF, $f(N)$, is defined as the number of lines per unit column density and per unit redshift absorption path, dX (Tytler 1987). The CDDF is a fundamental statistics for absorption lines, similar for many aspects to the luminosity function for stars and galaxies.

The redshift absorption path is used to remove the redshift dependence in the sample and put everything on a comoving coordinate scale. In the assumed cosmology, it is defined as

$$dX \equiv (1+z)^2[\Omega_{\rm m}(1+z)^3 + \Omega_\Lambda]^{-1/2} dz. \quad (1)$$

With the adopted definition, $f(N)$ does not evolve at any redshifts for a population whose physical size and comoving space density are constant.

We have computed $f(N)$ splitting our data into two redshift bins in order to have comparable $\Delta X_{\rm tot}$ in both of them: $4.35 < z < 5.3$ ($\Delta X_{\rm tot} = 20.893$) and $5.3 < z < 6.2$ ($\Delta X_{\rm tot} = 19.526$), considering column densities $12.6 \leq \log N({\rm C\,IV}) \leq 15$. The possible evolution with redshift of the CDDF has been verified by comparing $f(N)$ for the present data with $f(N)$ for the lower redshift sample in D'Odorico et al. (2010). Due to the higher resolution of the spectra in the latter work, C IV lines with velocity separation smaller than 50 km s^{-1} have been merged into C IV systems.

The result is shown in Fig. 18, where $f(N)$ is plotted for four redshift intervals: $1.5 < z < 2.5$, $2.5 < z < 4$, $4.35 < z < 5.3$ and $5.3 < z < 6.2$ binned at $10^{0.4}$ N(C IV) cm^{-2}. The two CDDFs at higher redshift are complete starting from larger column densities, and a constant decrease with increasing redshift is observed in the bin corresponding to $14.2 < \log N({\rm C\,IV}) < 14.6$.

To quantify the redshift evolution of the CDDF, we have computed a least-squares fit of the four samples with a power law of the form $f(N) = BN^{-\alpha}$ (see Fig. 18). From the fit, we observe that in the highest redshift bin, the CDDF is lower by a factor of ∼3–4 with respect to the CDDF at $2.5 < z < 4$ and $4.35 < z < 5.3$. This is in good agreement with the result by Becker et al. (2009) which was based on NIRSPEC spectra at $R \approx 13\,000$ of four $z \sim 6$ QSOs, two of which are also in our sample. The CDDF in the lowest redshift bin has a different slope due to the presence of a larger number of absorption systems in the column density range $\log N({\rm C\,IV}) > 14.2$. At $\log N({\rm C\,IV}) = 14.4$, there is a factor of 7.5 difference between the CDDF at $1.5 < z < 2.5$ and that at $5.3 < z < 6.2$. Due to the small number of points, the power-law fit with two variables gives very large errors, in particular for the power-law normalization (highly correlated with the index errors). To obtain more solid results, we have tried also a power-law fit with a pivot column density, $f(N) = f(N_0)(N/N_0)^{-\alpha}$, where we chose $\log N_0 = 13.64$. The results of this fit are shown in Fig. 19. The power-law indices are lower than in the previous fit, although always consistent within $3\,\sigma$. The net decrease of the highest redshift CDDF is less evident but still present: there is a factor of ∼2−3 difference between the CDDF in the redshift bins $4.35 < z < 5.3$ and $5.3 < z < 6.2$.

5.2 The redshift evolution of the cosmic mass density of C IV

The CDDF can be integrated in order to obtain the cosmological mass density of C IV in QSO absorption systems as a fraction of the critical density today:

$$\Omega_{\rm C\,IV} = \frac{H_0\, m_{\rm C\,IV}}{c\, \rho_{\rm crit}} \int N f(N) {\rm d}N, \quad (2)$$

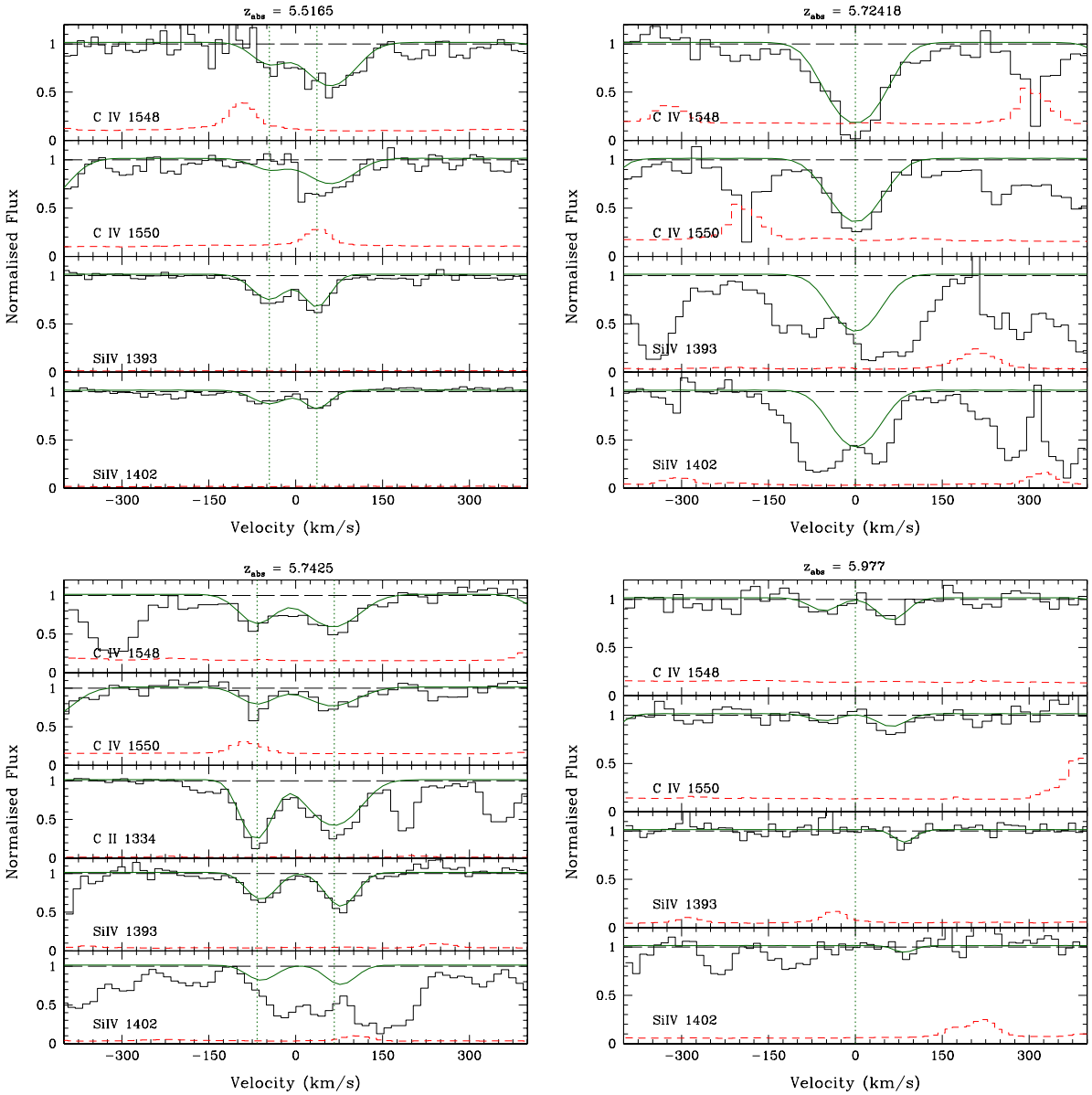

Figure 10. Detected C IV absorption systems with the associated Si IV doublets at $z_{\rm abs} > 5$ in the spectrum of SDSS J1030+0524. The strong absorption lines blended with the Si IV doublets at $z_{\rm abs} = 5.724\,18$ and 5.7425 are telluric lines that we could not correct.

where $H_0 = 100\,h$ km s^{-1} Mpc^{-1} is the Hubble constant, $m_{\rm C\,IV}$ is the mass of a C IV ion, c is the speed of light, $\rho_{\rm crit} = 1.88 \times 10^{-29}\,h^2$ g cm^{-3} and $f(N)$ is the CDDF. The above integral can be approximated by the sum

$$\Omega_{\rm C\,IV} = \frac{H_0\, m_{\rm C\,IV}}{c\,\rho_{\rm crit}} \frac{\sum_i N_i({\rm C\,IV})}{\Delta X}, \quad (3)$$

with an associated fractional variance

$$\left(\frac{\delta\Omega_{\rm C\,IV}}{\Omega_{\rm C\,IV}}\right)^2 = \frac{\sum_i [N_i({\rm C\,IV})]^2}{\left[\sum_i N_i({\rm C\,IV})\right]^2} \quad (4)$$

as proposed by Storrie-Lombardi, McMahon & Irwin (1996). Note that the errors determined with this formula could be underestimated, in particular in the case of small line samples. In D'Odorico et al. (2010), we found that errors on $\Omega_{\rm C\,IV}$ computed with a bootstrap technique were, at maximum, a factor of ∼1.5 larger than those estimated with equation (4). For a fair comparison with previous results, however, we report in Table 3 the errors computed with equation (4).

Great care has to be taken when comparing results obtained from different samples, since the values of $\Omega_{\rm C\,IV}$ significantly depend on the column density range over which the sum or the integration is carried out, and as a consequence on the resolution and SNR of the available spectra. To take this aspect into account, we have computed two sets of values to be compared consistently with different data in the literature: the first with $13.4 \leq \log N({\rm C\,IV}) \leq 15$ and the second with $13.8 \leq \log N({\rm C\,IV}) \leq 15$. The final results (reported in Table 3) are not corrected for completeness. We have computed the correction to $\Omega_{\rm C\,IV}$ due to the undetected C IV lines with column densities $\log N({\rm C\,IV}) \sim 13.4{-}13.5$ in the redshift bin $z = 5.3$–6.2, which results to be negligible, of the order of $\sim 6 \times 10^{-10}$.

The evolution with redshift of $\Omega_{\rm C\,IV}$ is shown in the two panels of Fig. 20. The determination based on our X-shooter sample has been split into two redshift bins $4.35 \leq z \leq 5.3$ and $5.3 \leq z \leq 6.2$, to

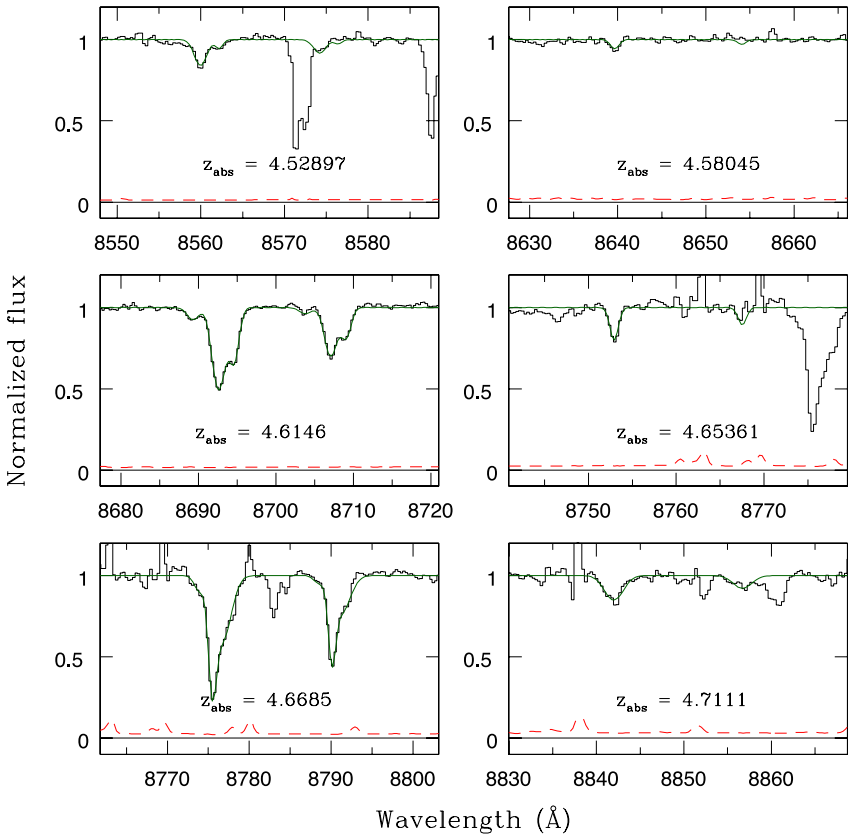

Figure 11. Detected C IV absorption systems in the spectrum of SDSS J1306+0356.

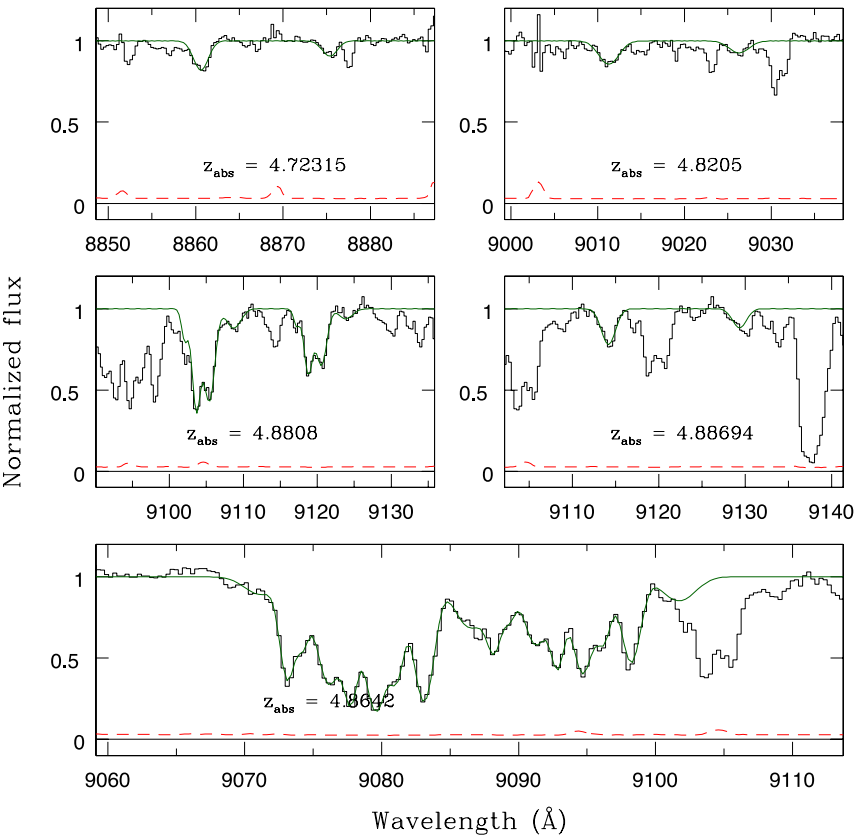

Figure 12. Detected C IV absorption systems in the spectrum of SDSS J1306+0356 (continuation of Fig. 11).

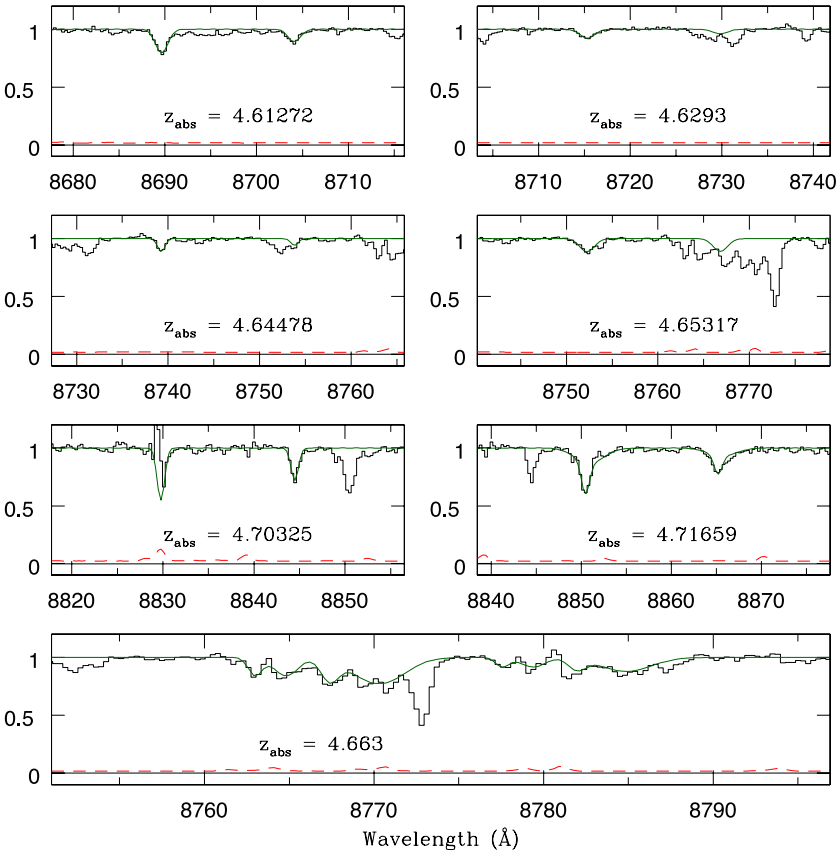

Figure 13. Detected C IV absorption systems in the spectrum of SDSS J1319+0950.

make a reliable comparison with the other most recent determination of $\Omega_{\rm C\,IV}$ at high redshift by Simcoe11. The behaviour of $\Omega_{\rm C\,IV}$ in the redshift range $1.5 \leq z \leq 4$ was determined with the high-resolution sample by D'Odorico et al. (2010). In the left plot, where $13.4 \leq \log N({\rm C\,IV}) \leq 15$, our measurement is compared with the result obtained by Simcoe11 using only the FIRE spectra, which have the same degree of completeness as our observations. We have not used their enlarged sample for which the completeness column density limit is not well defined. The two estimates are in very good agreement (within one sigma) as was expected since the two samples are almost identical. In the whole inspected redshift range, $\Omega_{\rm C\,IV}$ slowly increases from $z \sim 6.2$ to lower redshifts, and then it increases more steeply with a factor of ∼4 difference between $z \sim 3$ and $z \sim 1.5$.

The determination of $\Omega_{\rm C\,IV}$ was extended also to very low redshift ($z < 1$; Danforth & Shull 2008; Cooksey et al. 2010) using UV spectra at lower resolution and lower SNR limiting the detectability of C IV lines to larger column densities. In order to study the evolution of $\Omega_{\rm C\,IV}$ in the whole redshift range between $z \sim 0$ and 6.2, we have carried out a second computation of the values of $\Omega_{\rm C\,IV}$ for C IV systems in the column density range $13.8 \leq \log N({\rm C\,IV}) \leq 15$. The results are shown in the right plot of Fig. 20, where we have added also the results by D'Odorico et al. (2010) and the older determinations at high redshift by Pettini03 (corrected for the considered column density range), Ryan-Weber et al. (2009) and Becker et al. (2009). In this case, we compare our estimate of $\Omega_{\rm C\,IV}$ with the result obtained by Simcoe11 for their enlarged sample. Our point in the highest redshift bin is in agreement with all previous determinations. The value of $\Omega_{\rm C\,IV}$ in the redshift range $4.35 \leq z \leq 5.3$ is slightly lower than the estimate by Simcoe11, resulting in a smoother increase of the mass density towards lower redshifts. The discrepancy between our measurements and the result by Simcoe11 is due, in our opinion, to the fact that in Simcoe11 the two estimates at $4.35 \leq z \leq 5.3$ and at $5.3 \leq z \leq 6.2$ have different completeness limits. In the lower redshift range, the FIRE spectra are complete down to $N({\rm C\,IV}) \sim 13.4$, while the enlarged sample in the higher redshift bin is likely complete to higher column densities.

In summary, we observe a slow increase of the C IV content from $z \sim 6$ to $z \sim 1.5$ and then a flattening towards $z \sim 0$. Our data at high redshift together with the data points of D'Odorico et al. (2010) were fitted with the function: $\Omega_{\rm C\,IV} = (2 \pm 1) \times 10^{-8}[(1 + z)/4]^{-3.1 \pm 0.1}$ (see the right-hand panel of Fig. 20). Since we expect that these strong lines arise in the halo of star-forming galaxies (e.g. Adelberger et al. 2005), what we observe could be the effect of the progressive enrichment due to in situ star formation as the star formation rate density increases with time and then decreases below redshift ∼1.

6 REDSHIFT EVOLUTION OF IONIC RATIOS

It is generally thought that the IGM is kept ionized by the integrated UV emission from active nuclei and star-forming galaxies, but the relative contributions of these sources as a function of epoch are poorly known. At $z > 3$, the declining population of bright quasars appears to make an increasingly small contribution to the 1 Ryd radiation background (e.g. Bianchi, Cristiani & Kim 2001), and it is believed that massive stars in galactic and sub-galactic systems may provide the additional ionizing flux needed at early times (e.g., Madau, Haardt & Rees 1999; Gnedin 2000; Haehnelt et al. 2001;

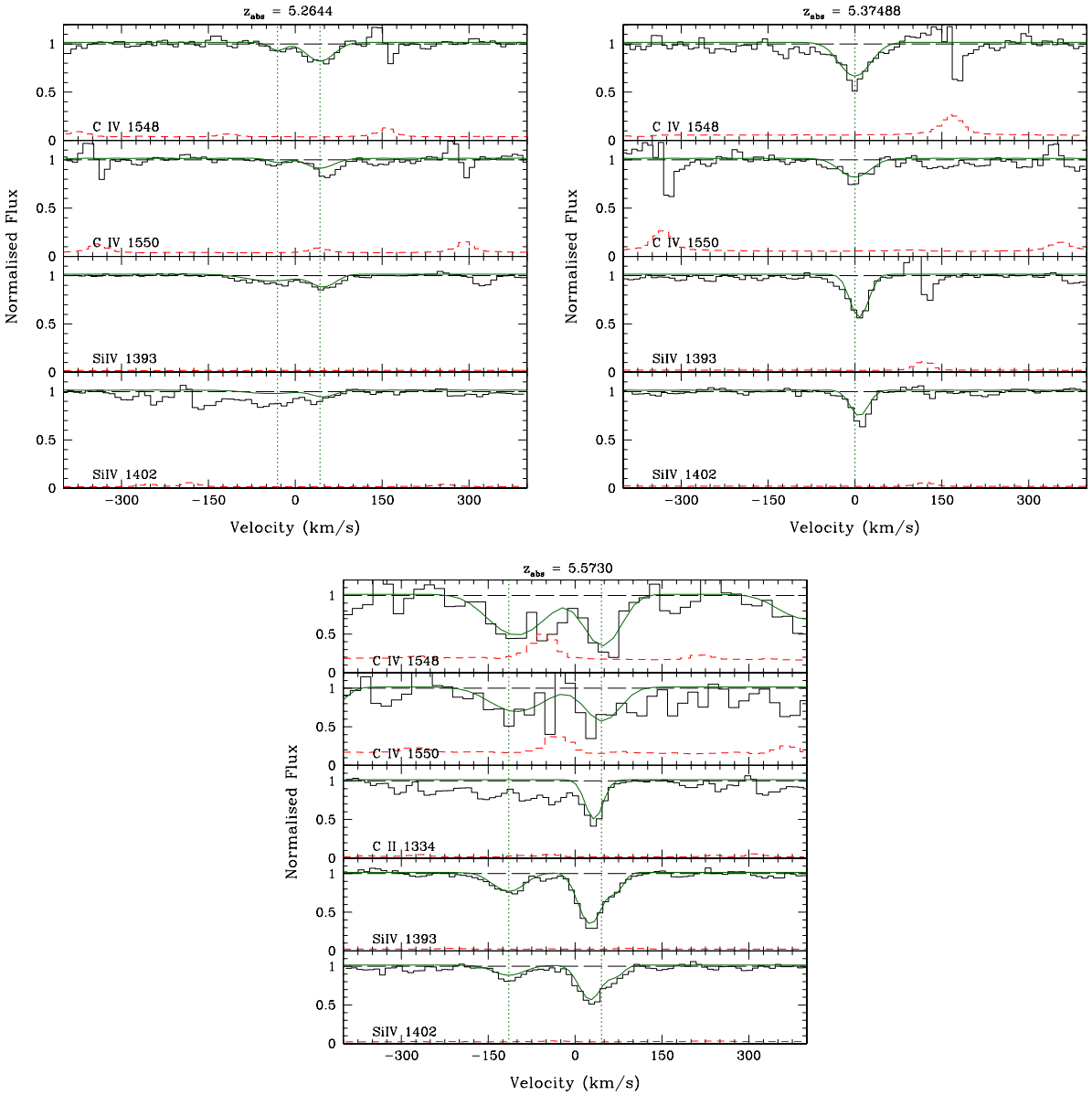

Figure 14. Detected C IV absorption systems with associated Si IV transitions at $z_{\rm abs} > 5$, in the spectrum of SDSS J1319+0950.

Wyithe & Loeb 2003; Meiksin 2005; Faucher-Giguère et al. 2008; Robertson et al. 2010). This idea may be supported by the detection of escaping ionizing radiation from individual Lyman break galaxies at $z \sim 3$ (but see Vanzella et al. 2012a,b).

The spectral shape of the ultraviolet background (UVB) radiation should be reflected into the ionization pattern of QSO metal system absorbers. In particular, the ionic ratios Si IV/C IV and C II/C IV are sensitive to the shape of the high-energy end of the ionizing spectrum where the He II break is expected (Giroux & Shull 1997; Savaglio et al. 1997; Agafonova et al. 2007; Bolton & Viel 2011).

In this work, we have detected for the first time a significant sample of Si IV doublets at $z \gtrsim 5$. This fact allows us to study the behaviour of the N(Si IV)/N(C IV) ratio for all those absorption systems in our sample for which both Si IV and C IV are outside the Lyα forest. The result is shown in Fig. 21, where this ionic ratio is plotted as a function of redshift, together with data from works at lower redshift (Savaglio et al. 1997; Songaila 1998; Boksenberg et al. 2003). In order to compare the data by Boksenberg et al. (2003), obtained from the fit of high-resolution HIRES@Keck spectra, with the other samples, we merged velocity components closer than 50 km s^{-1} before computing the Si IV/C IV ratios. Qualitatively, our X-shooter sample is characterized by large values and a small dispersion. Songaila (1998) claimed to observe a jump in the median value of the Si IV/C IV ratio at redshift ∼3 that she explained with a variation of the shape of the UVB spectrum due to the end of the He II re-ionization process. This result was not confirmed in the work by Kim, Cristiani & D'Odorico (2002). The authors of this work selected C IV systems in the range $1.6 < z < 3.6$ on the base of the associated H I absorber in order to consider only metals associated with Lyα forest lines. Also Boksenberg et al. (2003) found that the median values of Si IV/C IV obtained from summed column densities in systems are consistent with being constant over the whole observed range $1.9 < z < 4.4$.

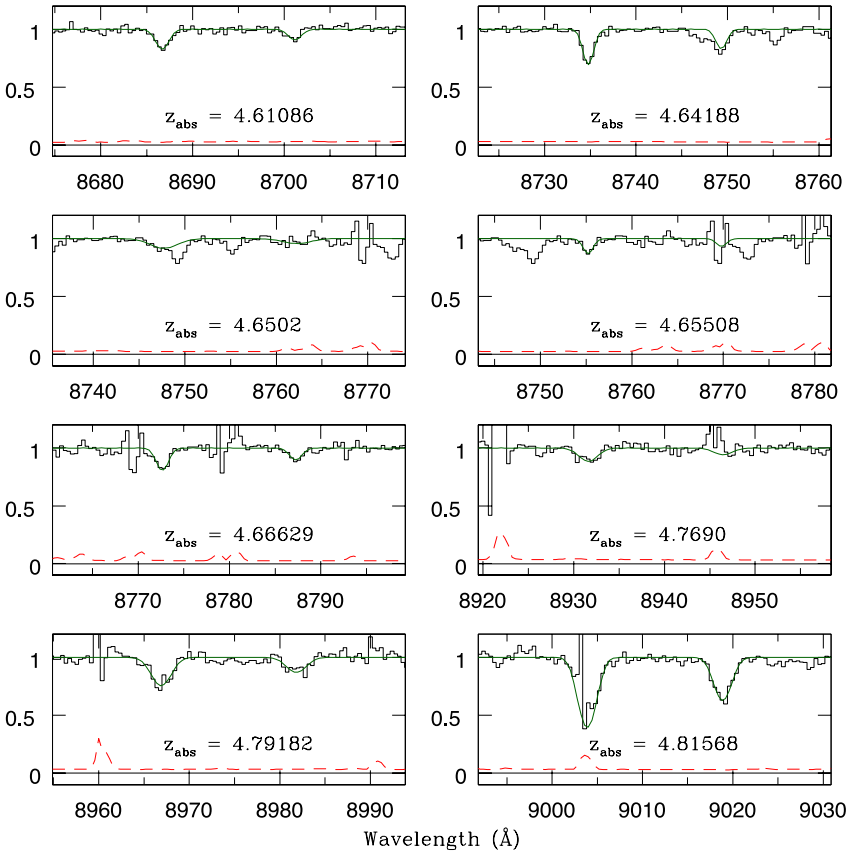

Figure 15. C IV absorption systems in the spectrum of SDSS J1509−1749.

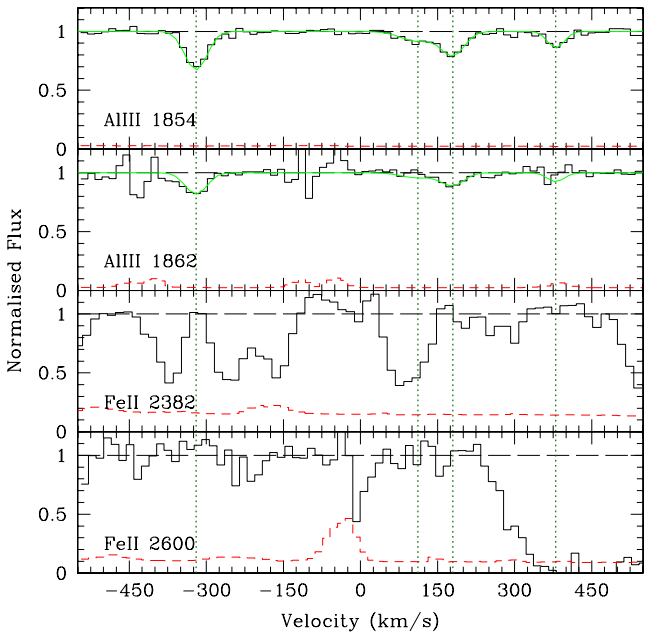

Figure 16. Possible complex Al III doublet at $z_{\rm abs} = 3.716$ in the spectrum of SDSS J1509−1749.

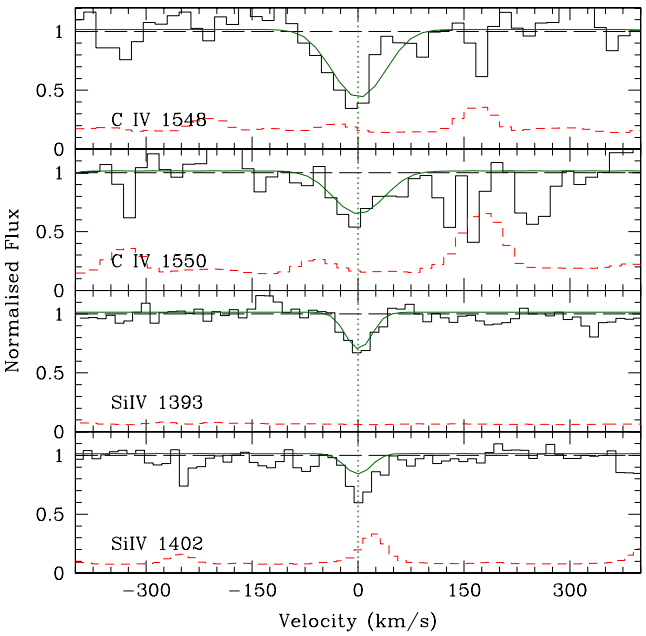

Figure 17. Absorption system at $z_{\rm abs} = 5.91572$ in the spectrum of SDSS J1509−1749.

A quantitative comparison of our sample with the lower redshift ones using the Kolmogorov–Smirnov test indicates that the X-shooter high-redshift sample is likely drawn from a different parent distribution. The cumulative distributions for the Si IV/C IV ratios of the three main samples are shown in Fig. 22. The probability that the X-shooter sample is drawn from the same distribution of the Songaila et al. sample or of the Boksenberg et al. one is tiny: $P = 1.3 \times 10^{-5}$ and 3×10^{-4}, respectively. The probability that the

Table 2. UVES observations.

QSO	z_{em}	J_{mag}	T_{exp} (s)	λ_{cen} (Å)	$\Delta z_{C\,IV}$
J1030+0524	6.308	18.87	15 300	7940	4.757−5.394
			22 600	814	
J1306+0356	6.016	18.77	12 219	7940	4.527−5.459
			6300	804	
			4277	814	
			9900	826	
			28 500	860	
J1044−0125	5.7824	18.31	5400	7940	4.343−5.365
			30 270	860	

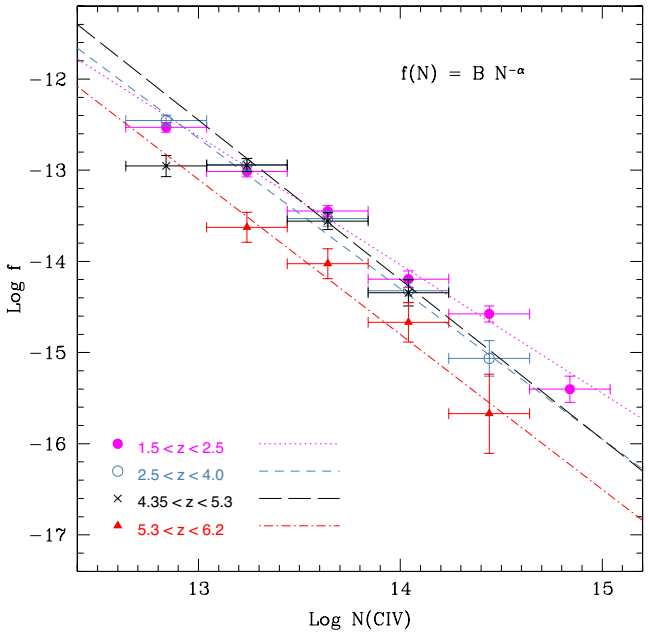

Figure 18. Comparison of the CDDF of C IV systems with $12.6 < \log N(\mathrm{C\,IV}) < 15$ in our sample ($4.35 < z < 6.2$) and in the lower redshift sample by D'Odorico et al. (2010) ($1.5 < z < 4$), where C IV lines closer than 50 km s^{-1} have been merged. Both redshift ranges were split into two smaller intervals: see the legend for the correspondence between the symbol and redshift interval. The bin size in $\log N(\mathrm{C\,IV})$ cm^{-2} is 0.4 and the error bars are $\pm 1\,\sigma$ based on the number of points in each bin. The lines are power laws of the form $f(N) = BN^{-\alpha}$ fitting the four samples with indices $\alpha = 1.41 \pm 0.07$, 1.65 ± 0.09, 1.75 ± 0.1 and 1.7 ± 0.2 in order of increasing redshift. See the legend for the correspondence between the line type and redshift interval.

two lower redshift samples are drawn from the same distribution is significantly larger: $P = 6 \times 10^{-2}$.

6.1 Photoionization models

We have run a set of ionization models with version 10.00 of the CLOUDY code, last described by Ferland et al. (1998). It is not conceivable to constrain the whole set of parameters of a photoionization model with just a few ionic transitions as in our case, due to the high level of degeneracy between e.g. total metallicity and chemical composition, or density and intensity of the ionizing flux. For this reason, we decided to run a limited set of models with parameters varying in reasonable ranges with the main aim of verifying that their predictions were compatible with the observed ionic column

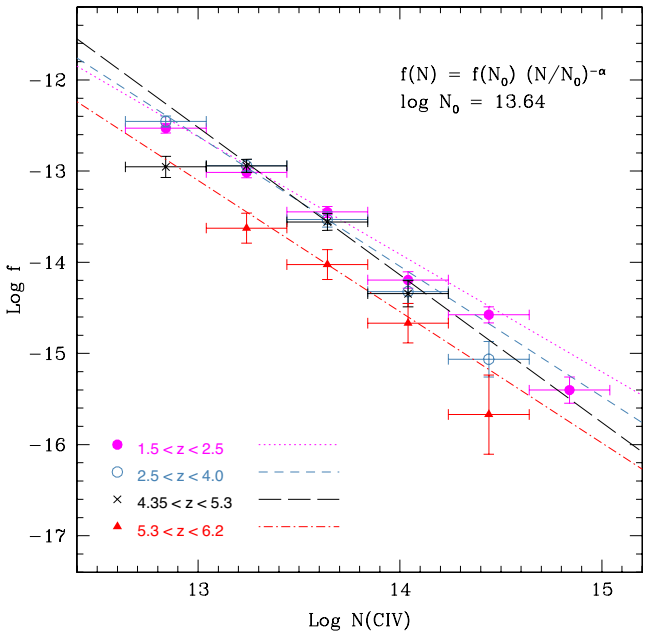

Figure 19. Same as Fig. 18 where the different redshift samples have been fitted with a power law of the form $f(N) = f(N_0)(N/N_0)^{-\alpha}$ and $N_0 = 10^{13.64}$. In this case, the exponential indices are $\alpha = 1.29 \pm 0.05$, 1.43 ± 0.06, 1.62 ± 0.2 and 1.44 ± 0.3 in order of increasing redshift. See the legend for the correspondence between the symbol type, line type and redshift interval.

Table 3. Values of $\Omega_{\mathrm{C\,IV}}$ for the X-shooter sample in two column density ranges.

z range	z_{med}	ΔX	Lines	$\Omega_{\mathrm{C\,IV}}$ ($\times 10^{-8}$)	$\delta\Omega$ ($\times 10^{-8}$)
$13.4 \leq \log N(\mathrm{C\,IV}) \leq 15$					
4.35−5.30	4.818	19.21	30	1.4	0.3
5.30−6.20	5.634	19.53	12	0.84	0.33
$13.8 \leq \log N(\mathrm{C\,IV}) \leq 15$					
4.35−5.30	4.802	19.21	9	0.65	0.22
5.30−6.20	5.706	19.53	5	0.61	0.32

densities. We chose the HM05 option in CLOUDY, which consists of a UVB made by quasars and galaxies with a 10 per cent photon escape fraction reprocessed by the IGM (Haardt & Madau 2001). Two sets of models were run: one at $z = 5.7$ to represent our data and one at $z = 3$ to represent the lower redshift sample. At each redshift, we considered two overdensities, $\delta \equiv \rho/\rho_0 - 1 = 10$ and 100, where ρ is the IGM baryonic density and ρ_0 is the mean density at the considered redshift; two metallicities, $[M/\mathrm{H}] = -2$ and -3, although in some cases also the predictions for $[M/\mathrm{H}] = -1$ are plotted, and two H I column densities, $\log N(\mathrm{H\,I}) = 16$ and 18. In all cases, solar relative abundances were adopted as a ground base. We ran also models with a relative abundance $[\mathrm{C/Si}] = -0.2$ as measured recently in metal-poor damped Lyman α systems (Cooke et al. 2011) and in $z > 5$ low-ionization absorption systems (Becker et al. 2012). The column densities of the interesting ions were changed by multiplying the intensity of the UVB spectrum by a factor ranging from 0.25 to 4 in steps of 0.25 (see Fig. 23).

Even assuming that C and Si are evolving in locksteps, their ratio could be affected not only by the ionization condition of the gas but also by the possible variation in the relative abundances of elements with respect to solar. In order to isolate ionization effects, we have

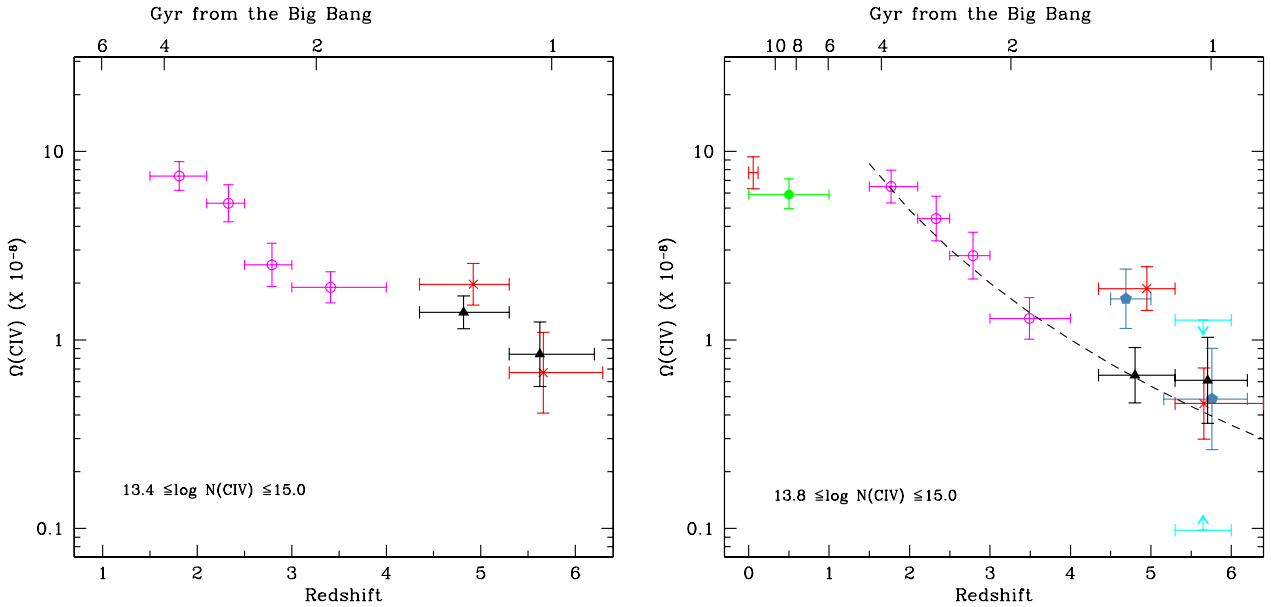

Figure 20. Evolution with redshift of the C IV cosmic mass density, $\Omega_{\rm C\,IV}$, computed for two column density ranges as specified in the figures. Left-hand panel: data points refer to this work (black triangles), Simcoe11 (red crosses) and D'Odorico et al. (2010, magenta open dots) for the C IV lines in the desired column density range. Right-hand panel: data points refer to this work (black triangles), Simcoe11 (red crosses) Pettini03 and Ryan-Weber et al. (2009, blue pentagons), Becker et al. (2009, cyan upper and lower limit 95 per cent confidence interval) D'Odorico et al. (2010, magenta open dots), Cooksey et al. (2010, green cross) and Danforth & Shull (2008, red plus). The dashed line denotes a fit to points with $z > 1.5$ (considering only our measurements in the range $z > 4.0$) of the form $\Omega_{\rm C\,IV} = (2 \pm 1) \times 10^{-8}[(1+z)/4]^{-3.1\pm0.1}$. The error bars are 1σ.

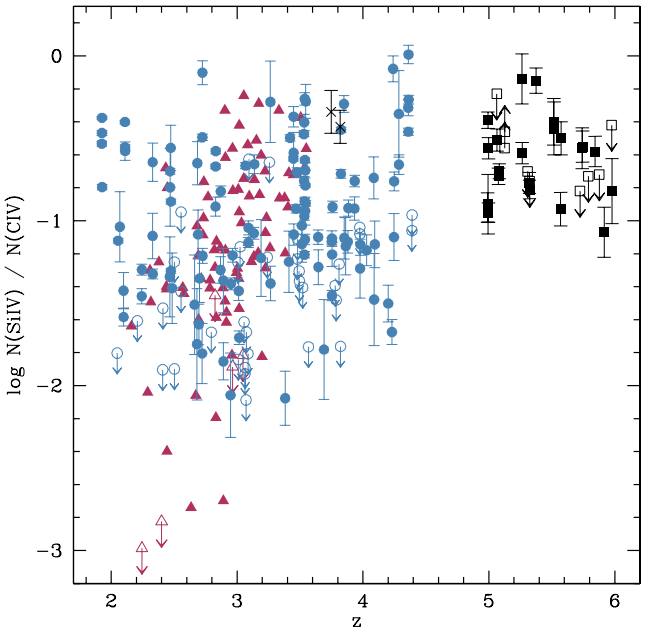

Figure 21. Evolution of the Si IV/C IV column density ratio as a function of redshift for the selected systems in our sample (black squares). The other data points are from Songaila (1998, triangles), Savaglio et al. (1997, crosses) and Boksenberg, Sargent & Rauch (2003, dots). The open symbols with arrows indicate upper or lower limits.

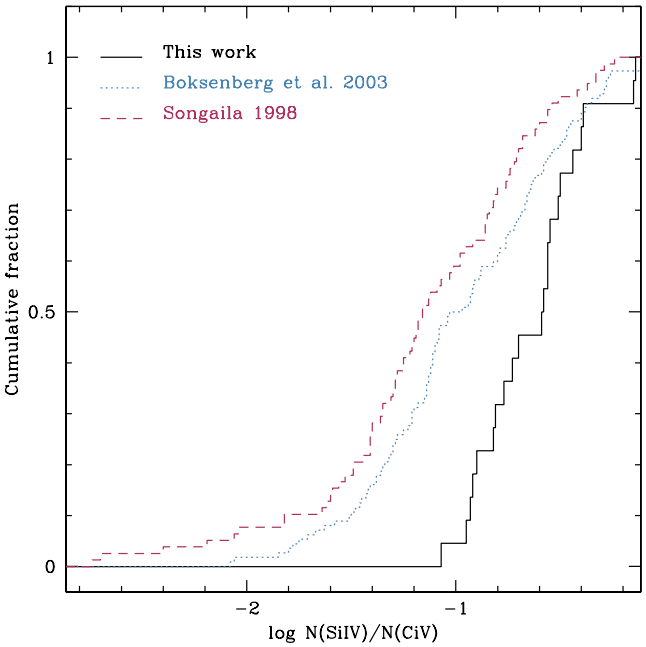

Figure 22. Cumulative distributions for the Si IV/C IV ratios of the three main samples used in the analysis: the X-shooter sample at $z \gtrsim 5$ (solid line) and the lower redshift samples of Songaila (1998, dashed line) and Boksenberg et al. (2003, dotted line).

looked for the C II 1334 Å lines associated with our C IV systems, which fall outside the Lyα forest. Only 12 systems in our sample satisfy this requirement, of which 7 are upper limits. The C II/C IV ratio is not affected by possible variation in the relative abundances of elements with respect to solar; on the other hand, the transition C II 1334 Å is saturated in most cases and the measured column density could be underestimated. Assuming that this is not the case for the five detections in our sample, we see from Fig. 24 that the measured column densities are, in general, larger than those measured at lower redshift for the same range of C IV column densities. This is evident also in Fig. 25, where most of the low-redshift data have a lower C II/C IV ratio with respect to our points.

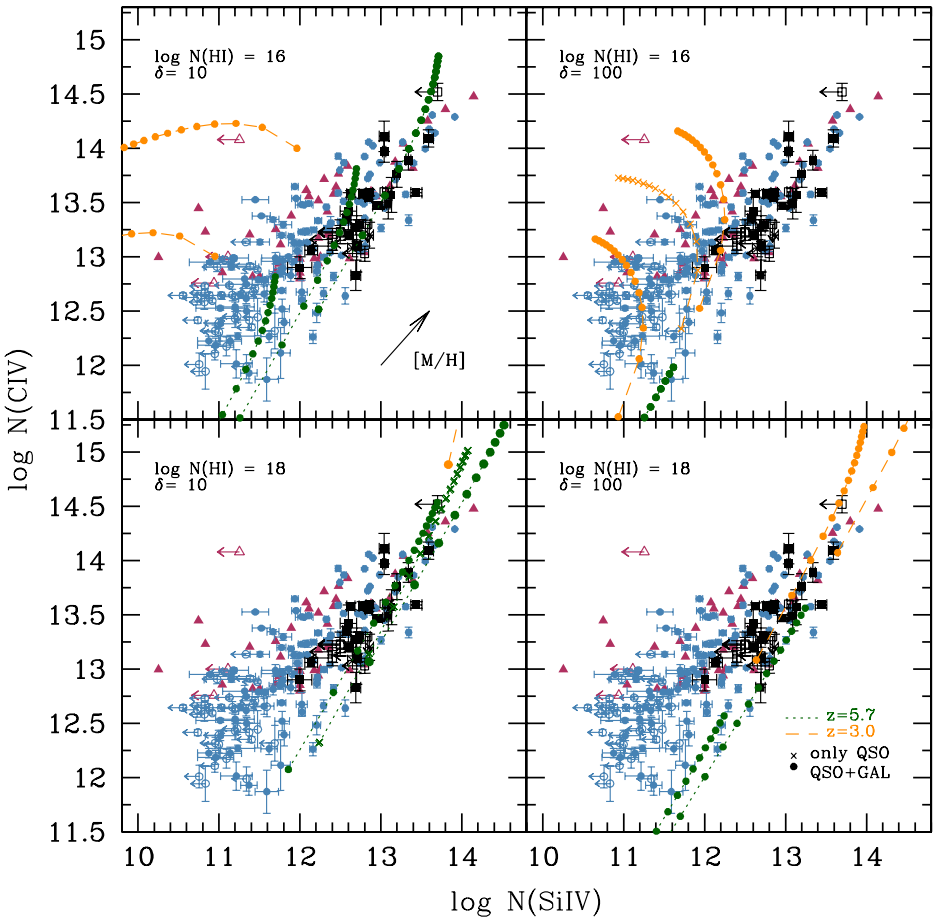

Figure 23. C IV column density as a function of the corresponding Si IV column density for all the systems of our sample (black squares). The other data points are from Savaglio et al. (1997, crosses), Songaila (1998, triangles) and Boksenberg et al. (2003, dots). The open symbols are limits. Superimposed are the CLOUDY models at $z = 5.7$ (green dotted lines) and $z = 3$ (orange dashed lines) with metallicities $[M/H] = -3$ and -2. In the upper-left panel, we show also the predictions at $z = 5.7$ for a metallicity $[M/H] = -1$. The arrow indicates approximately the direction of increasing metallicity. The predictions for a QSO-only background and $[M/H] = -2$ are shown in the lower-left panel (at $z = 5.7$) and in the upper-right panel (at $z = 3$). See the legend and the text for more details.

The comparison between observed data and CLOUDY models is shown in Figs 23–25. Each one of the four boxes present in every figure shows a different combination of δ and $\log N(\mathrm{H\,I})$ for the CLOUDY runs with the considered metallicities. In Fig. 25, we showed only the model results for $[M/H] = -2$, because the different metallicities give very similar results. When the model track is not shown in the figure, it is because it falls outside the plotted range of values. In the upper-right and bottom-left plots of Figs 23 and 24, we show also the result of a model with a UVB due only to quasars and metallicity $[M/H] = -2$. At a fixed metallicity and UV intensity, the QSO-only background produces (a factor of $\sim$2–4) less C II, C IV and Si IV with respect to the QSO–galaxy background; this effect is more evident at $z = 5.7$ where the contribution of QSOs to the UVB is less important.

Some qualitative considerations can be drawn as follows: the high-redshift absorbers are better explained by gas with an overdensity of 10 and an indicative total H I column density of $\log N(\mathrm{H\,I}) \sim 18$, while the lower redshift absorbers trace gas with $\delta \sim 100$ and preferentially have lower H I column density ($\log N(\mathrm{H\,I}) \sim 16$). This is in agreement with what was found in simulations (e.g. Oppenheimer & Davé 2006; Cen & Chisari 2011), where it is shown that C IV is a good tracer of the metallicity in the low-density gas at high redshift while becoming less and less representative going towards lower redshift where it traces gas at larger overdensities ($\sim$100). It has to be noted that the indication on the column density of absorbers could be an observational bias, since in our sample we are observing only the strongest systems due to the resolution and SNR of our spectra.

Models with a relative abundance [C/Si] $= -0.2$ do not reproduce the high-redshift data better than solar abundance model (see Fig. 25). This is somewhat puzzling since Becker et al. (2012) found this abundance result for a sample of absorption systems at $z > 5$ among which there are also the two absorption systems at $z_{\mathrm{abs}} \sim 5.7899$ and 5.8770 along the line of sight to J0818+1722. A possible explanation is that since those systems are likely damped or sub-damped Lyman α systems, they are subject to a local ionizing flux whose shape is different from the adopted one.

A more detailed analysis of the properties of the high-z absorbers will be carried out in a forthcoming paper with a set of cosmological hydro-simulations coupled with CLOUDY models.

7 CONCLUSIONS

The aim of this study was to investigate the metal content of QSO absorbers at very high redshift ($z > 4.35$) in the framework of the general picture of the enrichment history of the Universe.

The reported results are based on a programme devoted to the observations of QSOs at $z \sim 6$ with the X-shooter spectrograph

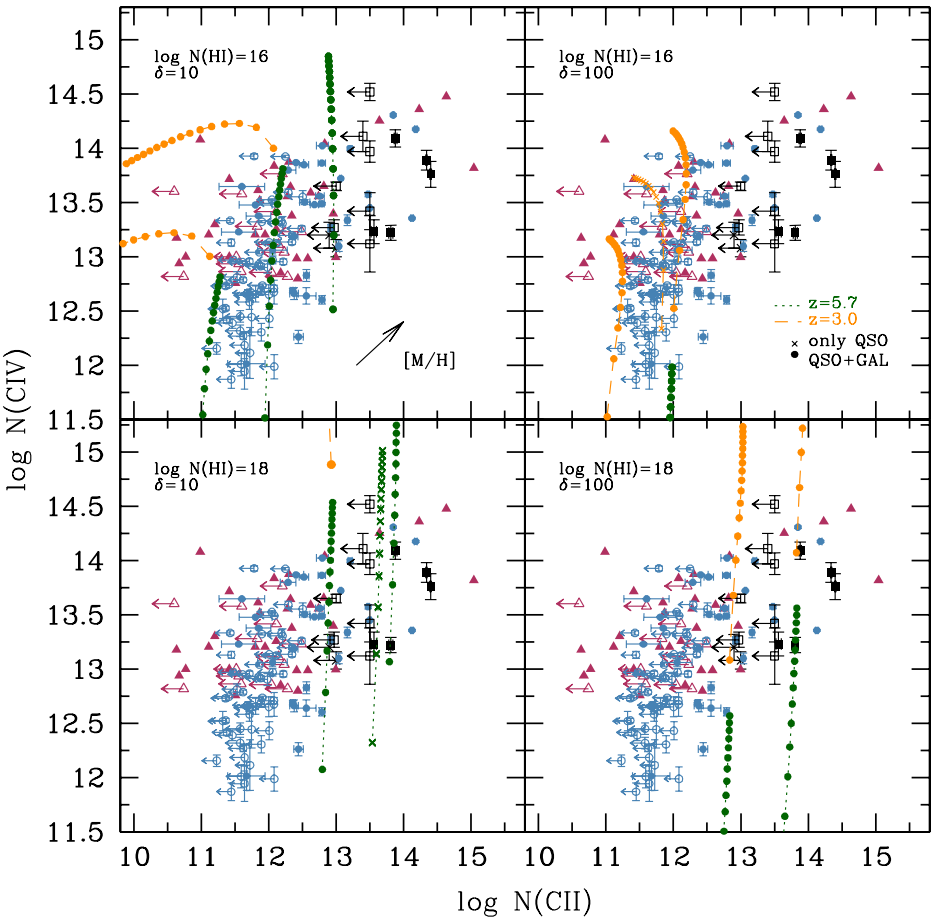

Figure 24. C IV column density as a function of the corresponding C II column density for the 12 systems in our sample with both transitions outside the Lyα forest (black and open squares). The other data points are from Savaglio et al. (1997, crosses), Songaila (1998, triangles) and Boksenberg et al. (2003, dots). The open symbols are limits. Superimposed are the CLOUDY models. In the upper-left panel, we show also the predictions at $z = 5.7$ for a metallicity $[M/H] = -1$. The arrow indicates approximately the direction of increasing metallicity. The predictions for a QSO-only background and $[M/H] = -2$ are shown in the lower-left panel (at $z = 5.7$) and in the upper-right panel (at $z = 3$). See the legend and the text for more details.

at the unit 2 of the ESO VLT telescope. The final sample consists of the spectra of six objects, of which four were observed in our programme and two were downloaded from the X-shooter archive. Each QSO spectrum was inspected to look for metal absorption lines outside the Lyα forest. Then, we focused our attention on the properties of the C IV sample looking, in particular, for the presence of the associated Si IV doublet and C II 1334 Å line. A total of 102 C IV lines were detected in the redshift interval $4.35 < z < 6.2$, of which 25 with $z \gtrsim 5$ have associated Si IV and 5 show the C II line. This is the first time that a significant sample of $z \gtrsim 5$ Si IV doublets is reported.

We have reduced and analysed also the UVES spectra of $z \sim 6$ QSOs that were available in the archive. Unfortunately, those observations have too low signal-to-noise ratio to add significant information to the X-shooter observations. In a few cases, thanks to the higher resolution, it was possible to discard the weak metal systems detected with X-shooter.

The main results are described in the following.

(i) C IV *CDDF*: the data sample has been divided into two redshift bins. The CDDF for the bin at $4.35 < z < 5.3$ is in good agreement with the CDDF of the low-redshift systems ($1.5 < z < 4$). On the other hand, the distribution function of the lines in the high-redshift bin ($5.3 < z < 6.2$) shows systematically lower values in all four column density bins, by a factor of ∼2–4 depending on the considered fitting function. This indicates that the properties (e.g. the number density or the physical size) of the C IV absorber population are varying at those redshifts. The observed decrease at $z > 5.3$ is in agreement with what was found by Becker et al. (2009) with a sample of four QSOs observed at slightly higher resolution.

(ii) C IV *cosmic mass density*: the contribution of C IV lines to the cosmic mass density has been computed for our line sample and compared with previous results at lower and similar redshift. We considered two column density regimes which give slightly different results (see Table 3). $\Omega_{\rm C\,IV}$ computed for the absorption lines with $13.4 \leq \log N({\rm C\,IV}) \leq 15$ is in very good agreement with the recent determination by Simcoe11. We observe a slow increase from the range $5.3 < z < 6.2$ to $4.35 < z < 5.3$ and then to $3 < z < 4$, then the mass density evolves more steeply with an increase of a factor of ∼4 to $z \simeq 1.5$. Considering the evolution in time, we see approximately an increase of a factor of ∼2 in $\Omega_{\rm C\,IV}$ every Gyr. In the case of the stronger C IV lines ($13.8 \leq \log N({\rm C\,IV}) \leq 15$), a gentle rise of a factor of ∼10 is observed between $z \simeq 6.2$ and $z \simeq 1.5$ with a possible flattening towards $z \sim 0$. For the strong lines, we do not observe a drop in $\Omega_{\rm C\,IV}$ between $\langle z \rangle = 4.802$ and 5.725 as claimed by other authors (Ryan-Weber et al. e.g. 2009; Simcoe11). The increase between $z \sim 6.2$ and 1.5 is well fitted by a power law: $\Omega_{\rm C\,IV} = (2 \pm 1) \times 10^{-8}[(1+z)/4]^{-3.1 \pm 0.1}$. The observed behaviour

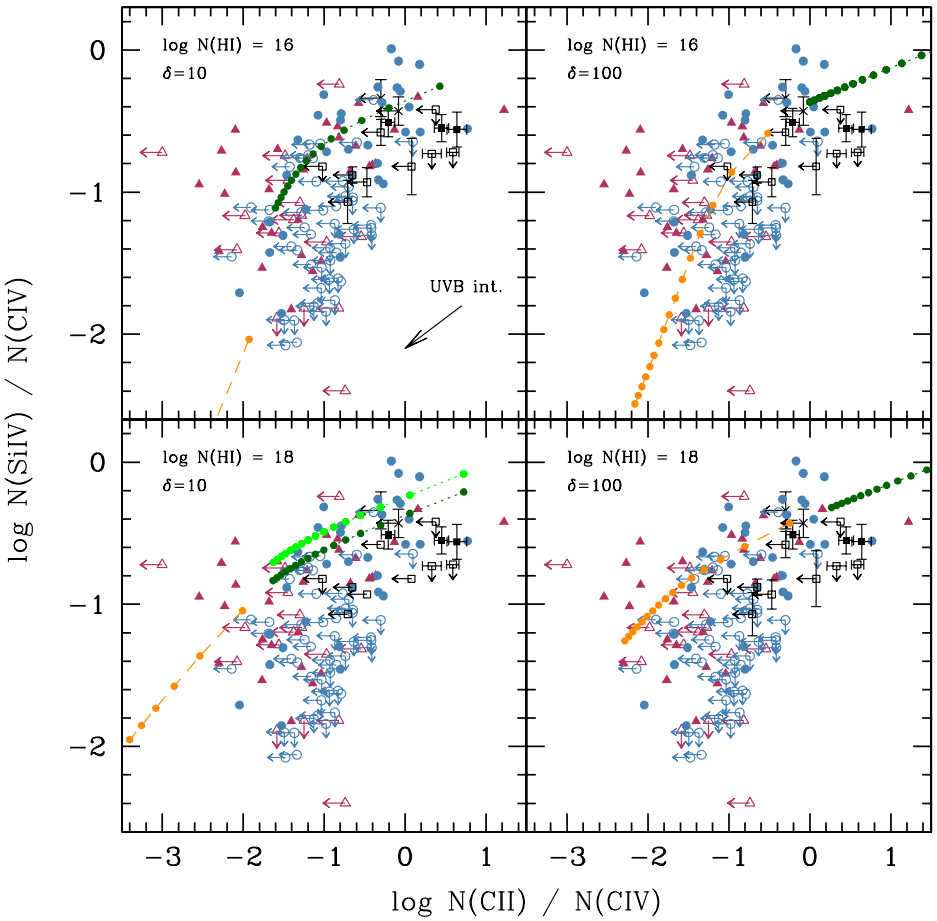

Figure 25. Si IV/C IV ionic ratio as a function of the C II/C IV ratio for the 12 systems in our sample for which all three transitions are outside the Lyα forest (black and open squares). The other data points are from Savaglio et al. (1997, crosses), Songaila (1998, triangles) and Boksenberg et al. (2003, dots). The open symbols are limits. Superimposed are the CLOUDY models for a metallicity $[M/H] = -2$. The model in light grey in the lower-left panel has a relative abundance $[C/Si] = -0.2$ for the gas at $z = 5.7$. The arrow indicates approximately the direction of increasing UVB intensity. See Fig. 24 for the legend of the models and the text for more details.

is suggestive of a progressive accumulation of the metals produced by stars inside galaxies in the circumgalactic medium and IGM. When the star formation rate density is observed to decrease, below $z \sim 1$, the increase in $\Omega_{\rm C\,IV}$ slows down. It is important to remember that the abundance of our observable, the triply ionized carbon, is determined by the total amount of carbon but also by the ionization conditions in the gas: cosmological simulations could help to fully interpret our results and determine the true evolution of the metal content in the IGM.

(iii) C IV, Si IV *and* C II *combined constraints on the nature of absorbers*: starting from our C IV sample, we built a subsample of lines with associated Si IV doublets and a further subsample of lines for which it was possible to detect both the Si IV and the C II 1334 Å lines, outside the Lyα forest. The Si IV/C IV column density ratios for our sample have a small dispersion around a logarithmic median value of -0.58. This is somewhat higher than the median value of ~ -1.2 at $z \sim 3$ found by Boksenberg et al. (2003). A Kolmogorov–Smirnov test run on our sample in comparison with lower redshift samples ($z \sim 3$) indicates that they are likely not drawn from the same parent distribution, suggesting a change in the ionization conditions of the gas with increasing redshift. A qualitative test was carried out by comparing the observed ionic column densities with the results of a (limited) set of CLOUDY ionization models. We adopt a Haardt–Madau UVB, solar abundances and metallicities $[M/H] = -2$ and -3. Indicatively, the observed C IV absorbers at high redshift are better explained by gas with overdensity of $\sim$10, while at $z \sim 3$ better agreement is obtained with gas with $\delta \simeq 100$. This is in agreement with the predictions of metal enrichment simulations (e.g. Oppenheimer & Davé 2006; Cen & Chisari 2011). CLOUDY models with $[C/Si] = -0.2$ give a worse representation of the high-redshift data although this relative abundance was obtained for $z > 5$ absorption systems. This discrepancy suggests that probably some of these absorbers trace very dense and neutral environments ionized by local sources.

The present study shows how metal-enriched ionized gas is present even at very high redshift possibly in the form of dense systems affected by the presence of local ionizing stellar sources. Unfortunately, the modest number of lines of sight and the relatively low SNR in the NIR region are still preventing us to reach solid results on the statistics of C IV absorbers at $z > 5$. Only a major observational effort could improve significantly this situation due to the faintness of the targets and their paucity. This will be an extremely interesting and driving science case for the next generation of visual and NIR high-resolution spectrographs at the Extremely Large Telescopes (ELTs).

ACKNOWLEDGEMENTS

This work is supported by PRIN-INAF 2010. MV is supported by PRIN-MIUR, INFN/PD51 and the ERC Starting Grant CosmoIGM. We would like to thank the anonymous referee for the very careful reading of the paper and the helpful suggestions.

REFERENCES

Adelberger K. L., Shapley A. E., Steidel C. C., Pettini M., Erb D. K., Reddy N. A., 2005, ApJ, 629, 636
Agafonova I. I., Levshakov S. A., Reimers D., Fechner C., Tytler D., Simcoe R. A., Songaila A., 2007, A&A, 461, 893
Ballester P., Modigliani A., Boitquin O., Cristiani S., Hanuschik R., Kaufer A., Wolf S., 2000, The Messenger, 101, 31
Becker G. D., Sargent W. L. W., Rauch M., Simcoe A. R., 2006, ApJ, 640, 69
Becker G. D., Rauch M., Sargent W. L. W., 2009, ApJ, 698, 1010
Becker G. D., Sargent W. L. W., Rauch M., Calverley A. P., 2011, ApJ, 735, 93
Becker G. D., Sargent W. L. W., Rauch M., Carswell R. F., 2012, ApJ, 744, 91
Bianchi S., Cristiani S., Kim T., 2001, A&A, 376, 1
Boksenberg A., Sargent W. L. W., Rauch M., 2003, preprint (astro-ph/0307557) (BSR03)
Bolton J. S., Viel M., 2011, MNRAS, 414, 241
Cen R., Chisari N. E., 2011, ApJ, 731, 11
Choudhury T. R., Ferrara A., Gallerani S., 2008, MNRAS, 385, L58
Cooke R., Pettini M., Steidel C. C., Rudie G. C., Nissen P. E., 2011, MNRAS, 417, 1534
Cooksey K. L., Thom C., Prochaska J. X., Chen H-W., 2010, ApJ, 708, 868
Cooksey K. L., Kao M. M., Simcoe R. A., O'Meara J. M., Prochaska J. X., 2013, ApJ, 763, 37
D'Odorico V., Calura F., Cristiani S., Viel M., 2010, MNRAS, 401, 2715
D'Odorico V. et al., 2011, Astron. Nachr., 332, 315 (Paper I)
Danforth C. W., Shull J. M., 2008, ApJ, 679, 194
Dekker H., D'Odorico S., Kaufer A., Delabre B., Kotzlowski H., 2000, Proc. SPIE, 4008, 534
Díaz C. G., Ryan-Weber E. V., Cooke J., Pettini M., Madau P., 2011, MNRAS, 418, 820
Fan X., CarilliC L., Keating B., 2006, ARA&A, 44, 415
Fan X. et al., 2001, AJ, 122, 2833
Fan X. et al., 2006, AJ, 131, 1203
Faucher-Giguère C., Lidz A., Hernquist L., Zaldarriaga M., 2008, ApJ, 682, 9
Ferland G. J., Korista K. T., Verner D. A., Ferguson J. W., Kingdon J. B., Verner E. M., 1998, PASP, 110, 761
Fontana A., Ballester P., 1995, The Messenger, 80, 37
Giroux M. L., Shull J. M., 1997, AJ, 113, 1505
Gnedin N. Y., 2000, ApJ, 535, 530
Goldoni P., Royer F., Francois P., Horrobin M., Blanc G., Vernet J., Modigliani A., Larsen J., 2006, Proc. SPIE, 6269, 80
Gonzàlez V., Labbé I., Bouwens R. J., Illingworth G., Franx M., Kriek M., Brammer G. B., 2010, ApJ, 713, 115
Haardt F., Madau P., 2001, in Neumann D. M., Van J. T. T., eds, Proc. 36th Rencontres de Moriond, Clusters of Galaxies and the High Resdhift Universe Observed in X-rays: Recent Results of XMM-Newton and Chandra. CEA, Saclay, p. 64
Haehnelt M. G., Madau P., Kudritzki R., Haardt F., 2001, ApJ, 549, 151
Jiang L., Fan X., Vestergaard M., Kurk J. D., Walter F., Kelly B. C., Strauss M. A., 2007, AJ, 134, 1150
Kelson D. D., 2003, PASP, 115, 688
Kim T.-S., Cristiani S., D'Odorico S., 2002, A&A, 383, 747
Kurk J. D. et al., 2007, ApJ, 669, 32
Madau P., Haardt F., Rees M. J., 1999, ApJ, 514, 648
Madau P., Ferrara A., Rees M. J., 2001, ApJ, 555, 92
Mannucci F., Buttery H., Maiolino R., Marconi A., Pozzetti L., 2007, A&A, 461, 423
Meiksin A., 2005, MNRAS, 356, 596
Mortlock D. J. et al., 2009, A&A, 505, 97
Mortlock D. J. et al., 2011, Nat, 474, 616
Oppenheimer B. D., Davé R., 2006, MNRAS, 373, 1265
Pettini M., Madau P., Bolte M., Prochaska J. X., Ellison S. L., Fan X., 2003, ApJ, 594, 695 (Pettini03)
Robertson B. E., Ellis R. S., Dunlop J. S., McLure R. J., Stark D. P., 2010, Nat, 468, 49
Ryan-Weber E. V., Pettini M., Madau P., 2006, MNRAS, 371, L78
Ryan-Weber E. V., Pettini M., Madau P., Berkeley J. Z., 2009, MNRAS, 395, 1476
Savaglio S., Cristiani S., D'Odorico S., Fontana A., Giallongo E., Molaro P., 1997, A&A, 318, 347
Simcoe R. A., 2006, ApJ, 653, 977
Simcoe R. A. et al., 2010, Proc. SPIE, 7735, 38
Simcoe R. A. et al., 2011, ApJ, 743, 21 (Simcoe11)
Songaila A., 1998, AJ, 115, 2184
Songaila A., Cowie L. L., 2002, AJ, 123, 2183
Storrie-Lombardi L., McMahon R. G., Irwin M., 1996, MNRAS, 283, 79
Tescari E., Viel M., D'Odorico V., Cristiani S., Calura F., Borgani S., Tornatore L., 2011, MNRAS, 411, 826
Tytler D., 1987, ApJ, 321, 49
Vanzella E. et al., 2012a, MNRAS, 424, L54
Vanzella E. et al., 2012b, ApJ, 751, 70
Vernet J. et al., 2011, A&A, 536, 105
Willott C. J. et al., 2007, AJ, 134, 2435
Wyithe J. S. B., Loeb A., 2003, ApJ, 586, 693

APPENDIX A: C IV AND SI IV ABSORPTIONS IN THE X-SHOOTER SPECTRA OF THE QSOS AT $z_{em} \sim 6$

Table A1. C IV absorption systems in the spectrum of SDSS J0818+1722.

System	Ion	z	W_0 (Å)	b (km s^{-1})	$\log N$ (cm^{-2})
1	C IV 1548	4.462 98 ± 0.000 01	0.258 ± 0.004	27.3 ± 0.7	13.90 ± 0.01
	C IV 1550		0.115 ± 0.002		
2	C IV 1548	4.498 00 ± 0.000 01	0.054 ± 0.003	11 ± 1	13.16 ± 0.02
	C IV 1550b		<0.059 ± 0.003		
3	C IV 1548b	4.508 38 ± 0.000 04	>0.045 ± 0.003	31 ± 4	13.12 ± 0.03
	C IV 1550		0.039 ± 0.004		
4	C IV 1548	4.523 05 ± 0.000 04	0.080 ± 0.006	51 ± 4	13.28 ± 0.02
	C IV 1550		0.055 ± 0.004		
5	C IV 1548	4.552 25 ± 0.000 05	0.030 ± 0.003	21 ± 8	12.78 ± 0.05
	C IV 1550		0.020 ± 0.003		
6	C IV 1548	4.577 33 ± 0.000 06	0.016 ± 0.005	15	12.65 ± 0.07
	C IV 1550		0.013 ± 0.003		
7	C IV 1548b	4.620 25 ± 0.000 05	>0.050 ± 0.004	36 ± 5	13.09 ± 0.04
	C IV 1550		0.034 ± 0.004		
8	C IV 1548	4.627 02 ± 0.000 05	0.050 ± 0.005	30 ± 6	13.00 ± 0.04
	C IV 1550		0.030 ± 0.004		
9	C IV 1548m	4.7263	0.539 ± 0.008		
	C IV 1550m		0.316 ± 0.007		
9a	C IV	4.7252 ± 0.0001		29 ± 6	13.59 ± 0.08
9b	C IV	4.726 15 ± 0.000 05		15 ± 4	13.73 ± 0.07
9c	C IV	4.726 99 ± 0.000 05		18 ± 2	13.89 ± 0.03
10	C IV 1548	4.731 58 ± 0.000 03	0.225 ± 0.008	45 ± 2	13.70 ± 0.01
	C IV 1550s		0.12 ± 0.02		
11	C IV 1548	4.877 39 ± 0.000 04	0.070 ± 0.006	32 ± 4	13.20 ± 0.03
	C IV 1550		0.037 ± 0.005		
12	C IV 1548	4.9417 ± 0.0001	0.136 ± 0.009	87 ± 7	13.46 ± 0.03
	C IV 1550		0.06 ± 0.01		
13	C IV 1548	5.0623 ± 0.0001	0.045 ± 0.009	26 ± 7	13.03 ± 0.07
	C IV 1550s		0.040 ± 0.007		
	Si IV				<12.8
14	C IV 1548	5.064 67 ± 0.000 05	0.127 ± 0.008	45 ± 4	13.47 ± 0.03
	C IV 1550sb		0.14 ± 0.01		
	Si IV 1402		0.038 ± 0.006		12.96 ± 0.06
15	C IV 1548	5.076 29 ± 0.000 04	0.18 ± 0.01	38 ± 4	13.59 ± 0.03
	C IV 1550		0.11 ± 0.02		
	Si IV 1402		0.033 ± 0.003		12.86 ± 0.04
16	C IV 1548	5.082 41 ± 0.000 04	0.147 ± 0.009	37 ± 3	13.55 ± 0.02
	C IV 1550		0.126 ± 0.007		
	Si IV 1402		0.036 ± 0.003		12.85 ± 0.04
17	C IV 1548	5.3085 ± 0.0001	0.052 ± 0.009	31 ± 8	13.10 ± 0.07
	C IV 1550		0.05 ± 0.01		
	Si IV				<12.4
18	C IV 1548	5.322 26 ± 0.000 05	0.09 ± 0.01	22 ± 4	13.35 ± 0.04
	C IV 1550		0.07 ± 0.01		
	Si IV 1393		0.037 ± 0.004		12.58 ± 0.05
	Si IV 1402		0.011 ± 0.003		
19	C IV 1548s	5.3243 ± 0.0002	0.06 ± 0.02	33 ± 11	13.2 ± 0.1
	C IV 1550		0.036 ± 0.009		
	Si IV				<12.4
20	C IV 1548s	5.7899 ± 0.0002	0.08 ± 0.02	30 ± 14	13.2 ± 0.1
	C IV 1550s		0.04 ± 0.01		
	Si IV				<12.5
	C II 1334	5.789 09 ± 0.000 04		26 ± 2	13.56 ± 0.04
21	C IV 1548	5.8441 ± 0.0001	0.11 ± 0.02	35 ± 8	13.27 ± 0.07
	C IV 1550		0.04 ± 0.02		
	Si IV 1393		0.045 ± 0.007		12.69 ± 0.06
	Si IV 1402		0.023 ± 0.005		
	C II 1334				<13
22	C IV 1548s	5.8770 ± 0.0001	0.09 ± 0.02	16 ± 10	13.22 ± 0.07
	C IV 1550		0.031 ± 0.009		
	Si IV				<12.5
	C II 1334	5.876 44 ± 0.000 02		11.2 ± 0.8	13.81 ± 0.03

Notes. b: line blended with another absorption line; m: multiple components; s: line contaminated by a sky emission line; l: feature below 3σ detection.

Table A2. C IV absorption systems in the spectrum of SDSS J0836+0054.

System	Ion	z	W_0 (Å)	b (km s^{-1})	$\log N$ (cm^{-2})
1	C IV 1548	4.530 13 ± 0.000 03	0.048 ± 0.004	11 ± 3	13.08 ± 0.03
	C IV 1550b		<0.046 ± 0.004		
2	C IV 1548	4.611 95 ± 0.000 07	0.030 ± 0.006	18 ± 7	12.82 ± 0.08
	C IV 1550		0.017 ± 0.006		
3	C IV 1548	4.668 40 ± 0.000 05	0.028 ± 0.005	10 ± 5	12.82 ± 0.06
	C IV 1550		0.016 ± 0.005		
4	C IV 1548mb	4.6855	0.398 ± 0.008		
	C IV 1550m		0.189 ± 0.009		
4a	C IV	4.684 27 ± 0.000 04		29 ± 3	13.46 ± 0.04
4b	C IV	4.686 51 ± 0.000 04		44 ± 5	13.58 ± 0.03
5	C IV 1548b	4.6985 ± 0.0001	<0.040 ± 0.007	15	12.80 ± 0.07
	C IV 1550b		>0.021 ± 0.004		
6	C IV 1548	4.7733 ± 0.0001	0.041 ± 0.006	40 ± 9	12.96 ± 0.06
	C IV 1550		0.034 ± 0.006		
7	C IV 1548	4.990 48 ± 0.000 04	0.051 ± 0.006	26 ± 4	13.06 ± 0.04
	C IV 1550		0.024 ± 0.006		
	Si IV 1393		0.015 ± 0.003	17 ± 2	12.14 ± 0.08
	Si IV 1402l		0.005 ± 0.003		
8	C IV 1548	4.992 64 ± 0.000 03	0.060 ± 0.006	28 ± 3	13.10 ± 0.04
	C IV 1550		0.029 ± 0.004		
	Si IV 1393		0.052 ± 0.004	18 ± 2	12.71 ± 0.03
	Si IV 1402		0.028 ± 0.004		
9	C IV 1548	4.994 21 ± 0.000 09	0.044 ± 0.005	29 ± 10	12.90 ± 0.10
	C IV 1550		0.022 ± 0.005		
	Si IV 1393		0.011 ± 0.005	19 ± 6	12.0 ± 0.15
	Si IV 1402		0.006 ± 0.003		
10	C IV 1548m	4.9965	0.208 ± 0.006		
	C IV 1550m		0.130 ± 0.007		
	Si IV 1393m		0.083 ± 0.004		
	Si IV 1402m		0.066 ± 0.005		
10a	C IV	4.996 34 ± 0.000 06		52 ± 4	13.58 ± 0.03
	Si IV			34 ± 3	12.63 ± 0.05
10b	C IV	4.996 93 ± 0.000 02	10	13.29 ± 0.05	
	Si IV		10	12.73 ± 0.04	
11	C IV 1548b	5.124 87 ± 0.000 03	<0.211 ± 0.006	33	<13.60
	C IV 1550b		<0.234 ± 0.005		
	Si IV 1393		0.104 ± 0.004	33 ± 2	13.04 ± 0.02
	Si IV 1402		0.047 ± 0.005		
12	C IV 1548b	5.127 12 ± 0.000 03	<0.112 ± 0.007	20	<13.30
	C IV 1550b		<0.074 ± 0.004		
	Si IV 1393		0.073 ± 0.005	20 ± 2	12.84 ± 0.03
	Si IV 1402		0.019 ± 0.004		
13	C IV 1548	5.322 77 ± 0.000 04	0.17 ± 0.02	31 ± 4	13.65 ± 0.04
	C IV 1550		0.10 ± 0.01		
	Si IV 1393		0.050 ± 0.005		12.77 ± 0.04
	Si IV 1402s		0.005 ± 0.006		
	C II 1334				<13.00

Notes. b: line blended with another absorption line; m: multiple components; s: line contaminated by a sky emission line; l: feature below 3σ detection.

Table A3. C IV absorption systems in the spectrum of SDSS J1030+0524.

System	Ion	z	W_0 (Å)	b (km s^{-1})	$\log N$ (cm^{-2})
1	C IV 1548	4.766 71 ± 0.000 04	0.063 ± 0.006	36 ± 4	13.13 ± 0.03
	C IV 1550b		<0.076 ± 0.005		
2	C IV 1548b	4.7966 ± 0.0001	<0.097 ± 0.006	94 ± 12	13.30 ± 0.04
	C IV 1550l		0.008 ± 0.004		
3	C IV 1548b	4.799 31 ± 0.000 01	<0.128 ± 0.005	13 ± 2	13.37 ± 0.02
	C IV 1550		0.072 ± 0.004		
4	C IV 1548	4.801 07 ± 0.000 01	0.149 ± 0.005	19 ± 2	13.46 ± 0.01
	C IV 1550b		<0.377 ± 0.005		
5	C IV 1548	4.890 66 ± 0.000 03	0.086 ± 0.007	30 ± 4	13.21 ± 0.02
	C IV 1550		0.033 ± 0.007		
6	C IV 1548m	4.9482	0.31 ± 0.01		
	C IV 1550m		0.18 ± 0.01		
6a	C IV	4.947 09 ± 0.000 04		12 ± 4	13.22 ± 0.04
6b	C IV	4.948 49 ± 0.000 02		29 ± 2	13.77 ± 0.01
7	C IV 1548m	5.5172	0.39 ± 0.06		
	C IV 1550ms		0.22 ± 0.07		
	Si IV 1393m	5.5164	0.233 ± 0.006		
	Si IV 1402m		0.093 ± 0.007		
7a	C IV	5.515 53 ± 0.000 02		34	13.4 ± 0.2
	Si IV			34 ± 2	13.10 ± 0.01
7b	C IV	5.5178 ± 0.0001		51 ± 7	13.92 ± 0.05
	Si IV	5.517 30 ± 0.000 01		20 ± 1	13.13 ± 0.01
8	C IV 1548	5.724 19 ± 0.0001	0.75 ± 0.06	47 ± 8	14.52 ± 0.08
	C IV 1550		0.49 ± 0.05		
	Si IV				<13.7
	C II 1334				<13.5
9	C IV 1548m	5.7428	0.54 ± 0.05		
	C IV 1550m		0.25 ± 0.06		
	Si IV 1393m	5.7429	0.31 ± 0.02		
	Si IV 1402mb		<0.71 ± 0.03		
9a	C IV	5.741 16 ± 0.000 04		29 ± 3	13.8 ± 0.1
	Si IV				13.20 ± 0.03
	C II 1334	5.740 97 ± 0.000 01		25.2 ± 0.6	14.40 ± 0.01
9b	C IV	5.7440 ± 0.0002		29 ± 3	13.89 ± 0.09
	Si IV	5.744 25 ± 0.000 04		29 ± 3	13.34 ± 0.03
	C II 1334	5.743 99 ± 0.000 04		50.6 ± 0.8	14.34 ± 0.01
10	C IV 1548l	5.9757 ± 0.0004	0.05 ± 0.02	15	13.1 ± 0.3
	C IV 1550l		0.02 ± 0.02		
	Si IV				<12.7
	C II 1334				<13.5
11	C IV 1548l	5.9784 ± 0.0002	0.07 ± 0.03	15	13.4 ± 0.2
	C IV 1550l		0.08 ± 0.02		
	Si IV 1393l	5.978 96 ± 0.000 09	0.03 ± 0.01	15	12.6 ± 0.1
	Si IV 1402l		0.01 ± 0.01		
	C II 1334				<13.5

Notes. b: line blended with another absorption line; m: multiple components; s: line contaminated by a sky emission line; l: feature below 3σ detection.

Table A4. C IV absorption systems in the spectrum of SDSS J1306+0356.

System	Ion	z	W_0 (Å)	b (km s^{-1})	$\log N$ (cm^{-2})
1	C IV 1548m	4.5292	0.090 ± 0.004		
	C IV 1550mb		$>0.021 \pm 0.003$		
1a	C IV	$4.528\,97 \pm 0.000\,03$		32 ± 3	13.15 ± 0.02
1b	C IV	$4.530\,40 \pm 0.000\,07$		15	12.44 ± 0.07
2	C IV 1548	$4.580\,45 \pm 0.000\,07$	0.019 ± 0.003	16 ± 7	12.49 ± 0.08
	C IV 1550s		0.001 ± 0.002		
3	C IV 1548m	4.6149	0.384 ± 0.006		
	C IV 1550m		0.196 ± 0.006		
3a	C IV	$4.612\,52 \pm 0.000\,07$		32 ± 7	12.81 ± 0.06
3b	C IV	$4.614\,64 \pm 0.000\,02$		35 ± 2	13.79 ± 0.02
3c	C IV	$4.615\,91 \pm 0.000\,03$		25 ± 2	13.44 ± 0.03
4	C IV 1548	$4.653\,61 \pm 0.000\,03$	0.054 ± 0.005	16 ± 3	13.07 ± 0.04
	C IV 1550		0.016 ± 0.007		
5	C IV 1548m	4.6685	0.42 ± 0.01		
	C IV 1550m		0.234 ± 0.009		
5a	C IV	4.6671 ± 0.0001		22 ± 9	12.68 ± 0.25
5b	C IV	$4.668\,18 \pm 0.000\,01$		12 ± 2	13.84 ± 0.04
5c	C IV	4.6688 ± 0.0001		50 ± 6	13.82 ± 0.07
6	C IV 1548	$4.711\,13 \pm 0.000\,07$	0.085 ± 0.008	48 ± 6	13.27 ± 0.04
	C IV 1550b		$<0.046 \pm 0.008$		
7	C IV 1548b	$4.723\,15 \pm 0.000\,05$	$<0.083 \pm 0.007$	37 ± 4	13.26 ± 0.04
	C IV 1550		0.034 ± 0.006		
8	C IV 1548	$4.820\,48 \pm 0.000\,08$	0.092 ± 0.008	51 ± 7	13.27 ± 0.04
	C IV 1550		0.040 ± 0.006		
9	C IV 1548m	4.864	1.58 ± 0.01		
	C IV 1550m		1.125 ± 0.01		
9a	C IV	4.8591 ± 0.0003		50	13.14 ± 0.07
9b	C IV	$4.860\,43 \pm 0.000\,03$		18 ± 3	13.76 ± 0.03
9c	C IV	$4.861\,16 \pm 0.000\,05$		10 ± 0	13.33 ± 0.07
9d	C IV	$4.862\,38 \pm 0.000\,04$		33 ± 4	13.97 ± 0.04
9e	C IV	$4.863\,41 \pm 0.000\,03$		15 ± 2	13.91 ± 0.04
9f	C IV	$4.864\,59 \pm 0.000\,03$		27 ± 3	14.12 ± 0.03
9g	C IV	$4.865\,60 \pm 0.000\,04$		17 ± 2	13.72 ± 0.06
9h	C IV	$4.866\,86 \pm 0.000\,01$		25 ± 1	14.02 ± 0.01
9i	C IV	$4.869\,11 \pm 0.000\,06$		52 ± 5	13.60 ± 0.03
10	C IV 1548m	4.8806	0.51 ± 0.01		
	C IV 1550m		0.264 ± 0.008		
10a	C IV	$4.879\,12 \pm 0.000\,04$		10	13.00 ± 0.05
10b	C IV	$4.880\,13 \pm 0.000\,03$		17 ± 2	13.77 ± 0.03
10c	C IV	$4.881\,26 \pm 0.000\,04$		27 ± 3	13.80 ± 0.03
11	C IV 1548b	$4.883\,40 \pm 0.000\,08$	$<0.057 \pm 0.006$	41 ± 7	13.10 ± 0.05
	C IV 1550		0.019 ± 0.005		
12	C IV 1548	$4.886\,94 \pm 0.000\,04$	0.092 ± 0.006	33 ± 3	13.31 ± 0.03
	C IV 1550b		$<0.072 \pm 0.006$		

Notes. b: line blended with another absorption line; m: multiple components; s: line contaminated by a sky emission line; l: feature below 3σ detection.

Table A5. C IV absorption systems in the spectrum of ULAS J1319+0950.

System	Ion	z	W_0 (Å)	b (km s^{-1})	$\log N$ (cm^{-2})
1	C IV 1548	4.612 73 ± 0.000 03	0.078 ± 0.004	29 ± 2	13.24 ± 0.02
	C IV 1550		0.044 ± 0.004		
2	C IV 1548	4.629 31 ± 0.000 08	0.035 ± 0.004	36 ± 6	12.86 ± 0.06
	C IV 1550b		<0.069 ± 0.004		
3	C IV 1548	4.644 78 ± 0.000 04	0.023 ± 0.004	7 ± 4	12.72 ± 0.05
	C IV 1550b		<0.017 ± 0.002		
4	C IV 1548b	4.653 17 ± 0.000 05	0.043 ± 0.003	34 ± 5	13.01 ± 0.04
	C IV 1550b		<0.120 ± 0.004		
5	C IV 1548mb	4.663	0.34 ± 0.01		
	C IV 1550mb		<0.189 ± 0.008		
5a	C IV	4.660 10 ± 0.000 03		10	12.89 ± 0.05
5b	C IV	4.661 27 ± 0.000 05		29 ± 4	13.12 ± 0.05
5c	C IV	4.662 94 ± 0.000 03		18 ± 3	13.09 ± 0.05
5d	C IV	4.664 82 ± 0.000 06		68 ± 6	13.62 ± 0.03
6	C IV 1548s	4.703 25 ± 0.000 02	0.05 ± 0.01	10 ± 3	13.50 ± 0.03
	C IV 1550		0.061 ± 0.003		
7	C IV 1548m	4.7167	0.155 ± 0.008		
	C IV 1550m		0.111 ± 0.007		
7a	C IV	4.716 59 ± 0.000 02		13 ± 3	13.27 ± 0.05
7b	C IV	4.7169 ± 0.0001		74 ± 9	13.37 ± 0.05
8	C IV 1548m	5.2640	0.090 ± 0.009		
	C IV 1550ms		0.06 ± 0.01		
	Si IV 1393m		0.089 ± 0.005		
	Si IV 1402mb		<0.105 ± 0.004		
8a	C IV	5.2627 ± 0.0001		57 ± 10	12.83 ± 0.14
	Si IV				12.69 ± 0.06
8b	C IV	5.264 52 ± 0.000 06		24 ± 3	13.20 ± 0.05
	Si IV				12.61 ± 0.05
9	C IV 1548	5.374 88 ± 0.000 04	0.17 ± 0.01	32 ± 4	13.59 ± 0.03
	C IV 1550		0.08 ± 0.01		
	Si IV 1393m		0.111 ± 0.004		
	Si IV 1402m		0.074 ± 0.003		
9a	Si IV	5.374 27 ± 0.000 05		11 ± 6	12.32 ± 0.07
9b	Si IV	5.375 08 ± 0.000 01		10	13.17 ± 0.02
10	C IV 1548s	5.570 49 ± 0.000 03	0.4 ± 0.1	34 ± 3	13.97 ± 0.10
	C IV 1550s		0.28 ± 0.07		
	Si IV 1393		0.108 ± 0.006		13.04 ± 0.02
	Si IV 1402		0.062 ± 0.005		
	C II 1334				<13.5
11	C IV 1548s	5.5740 ± 0.0001	0.35 ± 0.06	36 ± 11	14.09 ± 0.08
	C IV 1550s		0.29 ± 0.05		
	Si IV 1393m	5.5739	0.238 ± 0.006		
	Si IV 1402m		0.178 ± 0.005		
	C II 1334	5.573 72 ± 0.000 01		12 ± 1	13.88 ± 0.02
11a	Si IV	5.573 58 ± 0.000 01		20 ± 1	13.52 ± 0.01
11b	Si IV	5.574 57 ± 0.000 03		10	12.71 ± 0.05

Table A6. C IV absorption systems in the spectrum of CFHQS J1509−1749.

System	Ion	z	W_0 (Å)	b (km s^{-1})	$\log N$ (cm^{-2})
1	C IV 1548	4.610 86 ± 0.000 04	0.072 ± 0.007	34 ± 5	13.31 ± 0.03
	C IV 1550		0.034 ± 0.007		
2	C IV 1548[a]	4.641 88 ± 0.000 03	0.105 ± 0.008	19 ± 3	13.39 ± 0.03
	C IV 1550b		>0.085 ± 0.007		
3	C IV 1548b[a]	4.6501 ± 0.0002	>0.033 ± 0.005	68 ± 15	13.15 ± 0.08
	C IV 1550s		0.03 ± 0.01		
4	C IV 1548[a]	4.655 08 ± 0.000 06	0.040 ± 0.005	16 ± 8	12.93 ± 0.06
	C IV 1550s		0.04 ± 0.01		
6	C IV 1548[a]	4.666 29 ± 0.000 04	0.08 ± 0.01	24 ± 4	13.21 ± 0.04
	C IV 1550		0.043 ± 0.006		
7	C IV 1548	4.7690 ± 0.0001	0.06 ± 0.01	44 ± 10	13.13 ± 0.08
	C IV 1550s		0.014 ± 0.006		
8	C IV 1548	4.791 82 ± 0.000 05	0.14 ± 0.01	46 ± 4	13.51 ± 0.03
	C IV 1550		0.073 ± 0.009		
9	C IV 1548s[b]	4.815 68 ± 0.000 03	0.24 ± 0.02	39 ± 3	13.98 ± 0.02
	C IV 1550		0.20 ± 0.01		
10	C IV 1548s[b]	5.915 72 ± 0.000 06	0.31 ± 0.06	18 ± 5	14.11 ± 0.14
	C IV 1550s		0.22 ± 0.06		
	Si IV 1393		0.09 ± 0.01	18 ± 5	13.04 ± 0.06
	Si IV 1402s		0.09 ± 0.04		
	C II 1334				<13.4

[a]We found an alternative identification for this line: it could be Al III at $z_{\rm abs} \simeq 3.71$. [b]The line could be saturated.

APPENDIX B: OTHER ABSORPTION SYSTEMS

B1 SDSS J0818+1722

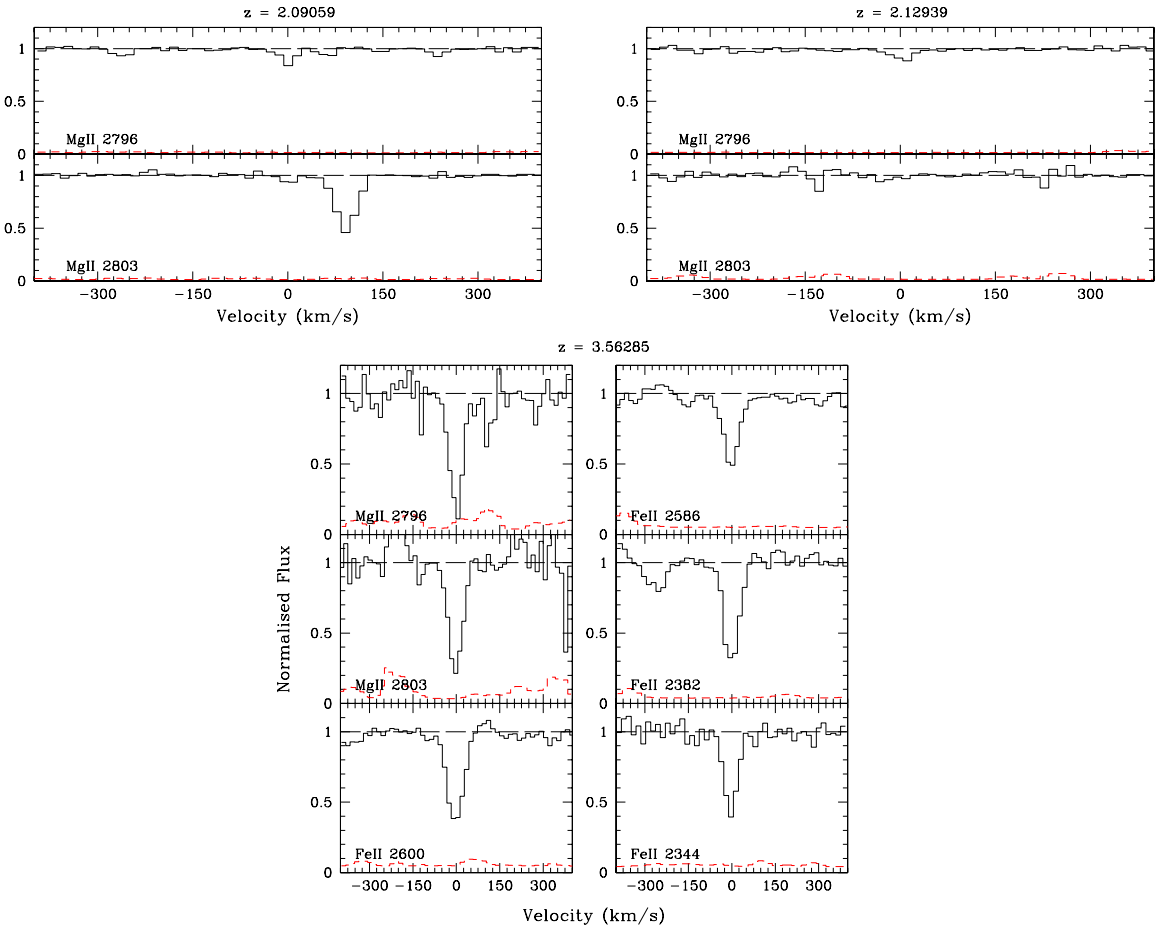

Figure B1. Mg II systems in the spectrum of SDSS J0818+1722.

B2 SDSS J0836+0054

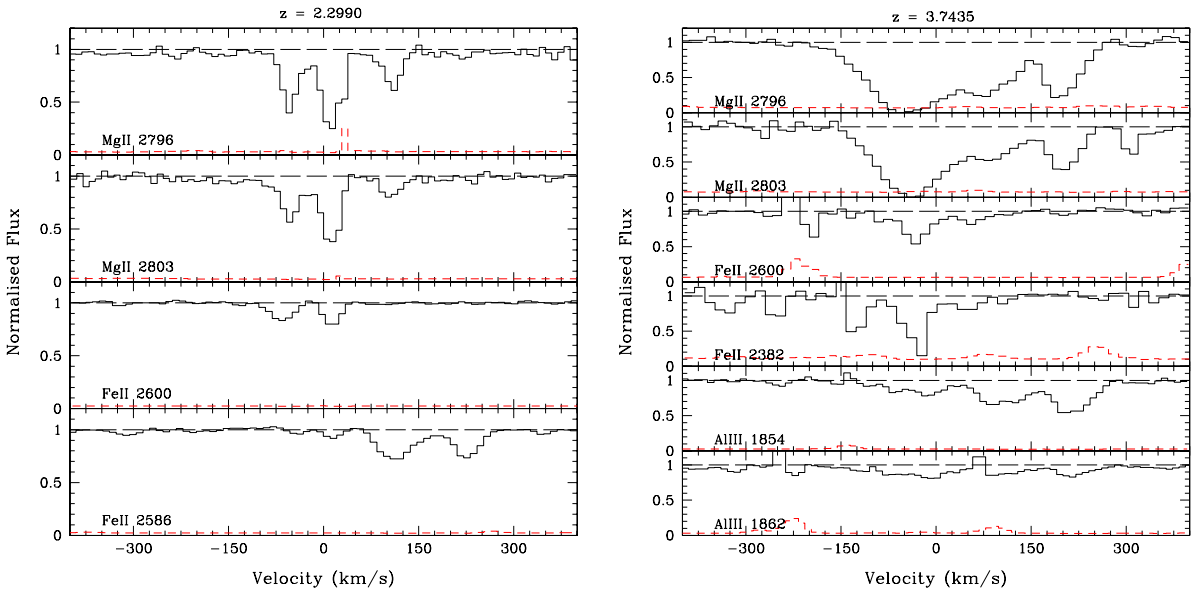

Figure B2. Mg II systems in the spectrum of SDSS J0836+0054.

B3 SDSS J1030+0524

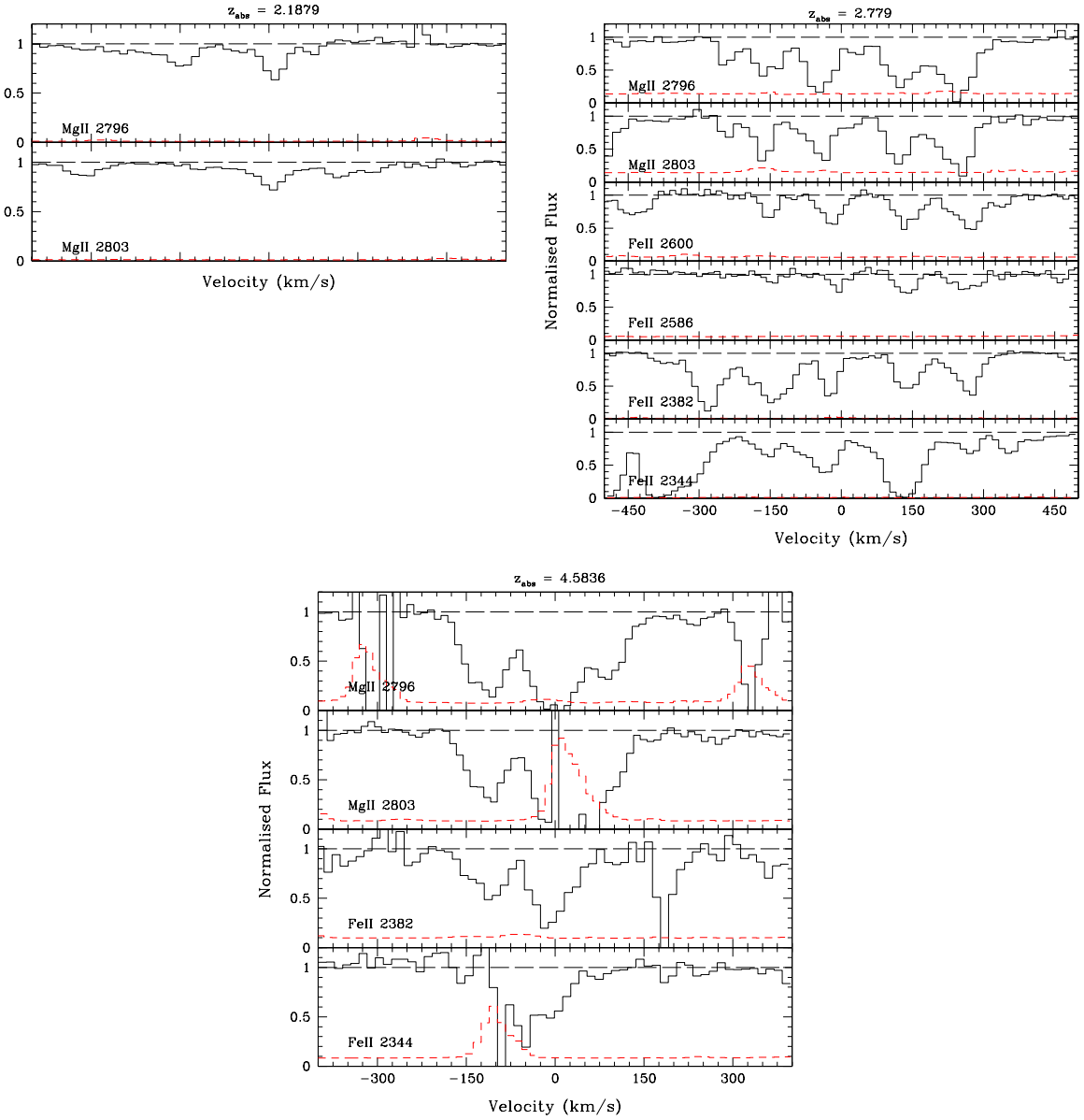

Figure B3. Mg II systems in the spectrum of SDSS J1030+0524.

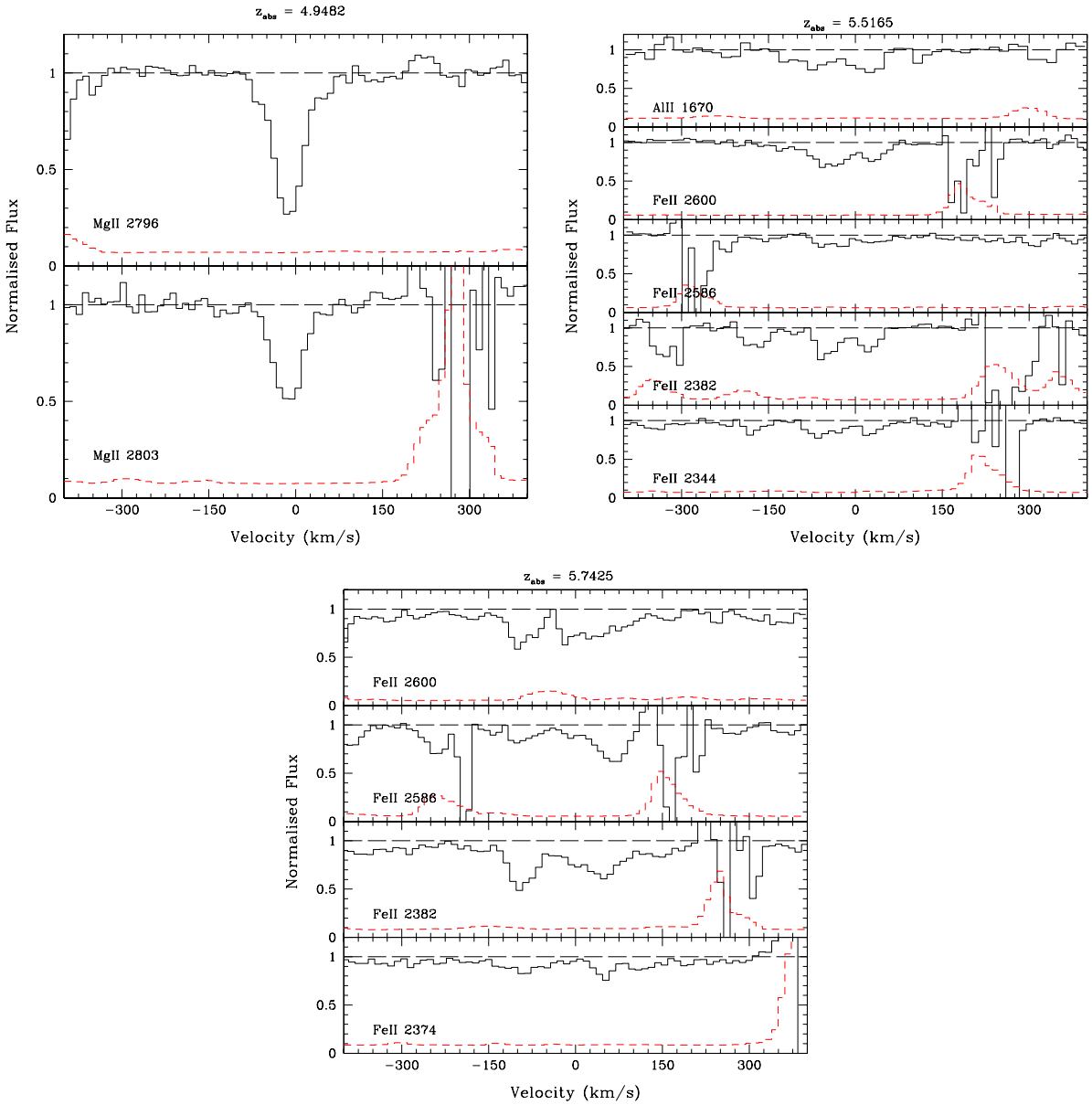

Figure B3 – *continued.*

B4 SDSS J1306+0356

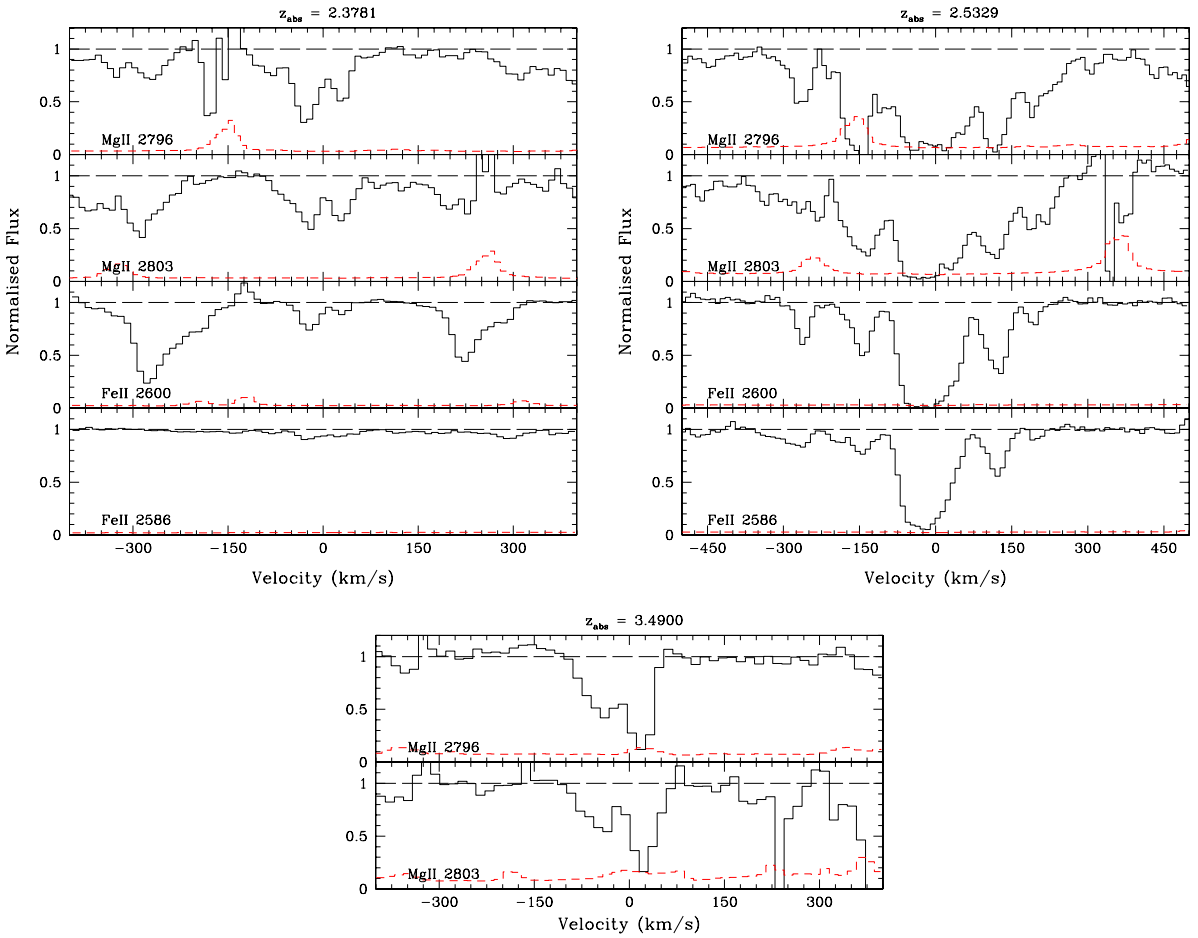

Figure B4. Mg II systems in the spectrum of SDSS J1306+0356.

B5 ULAS J1319+0950

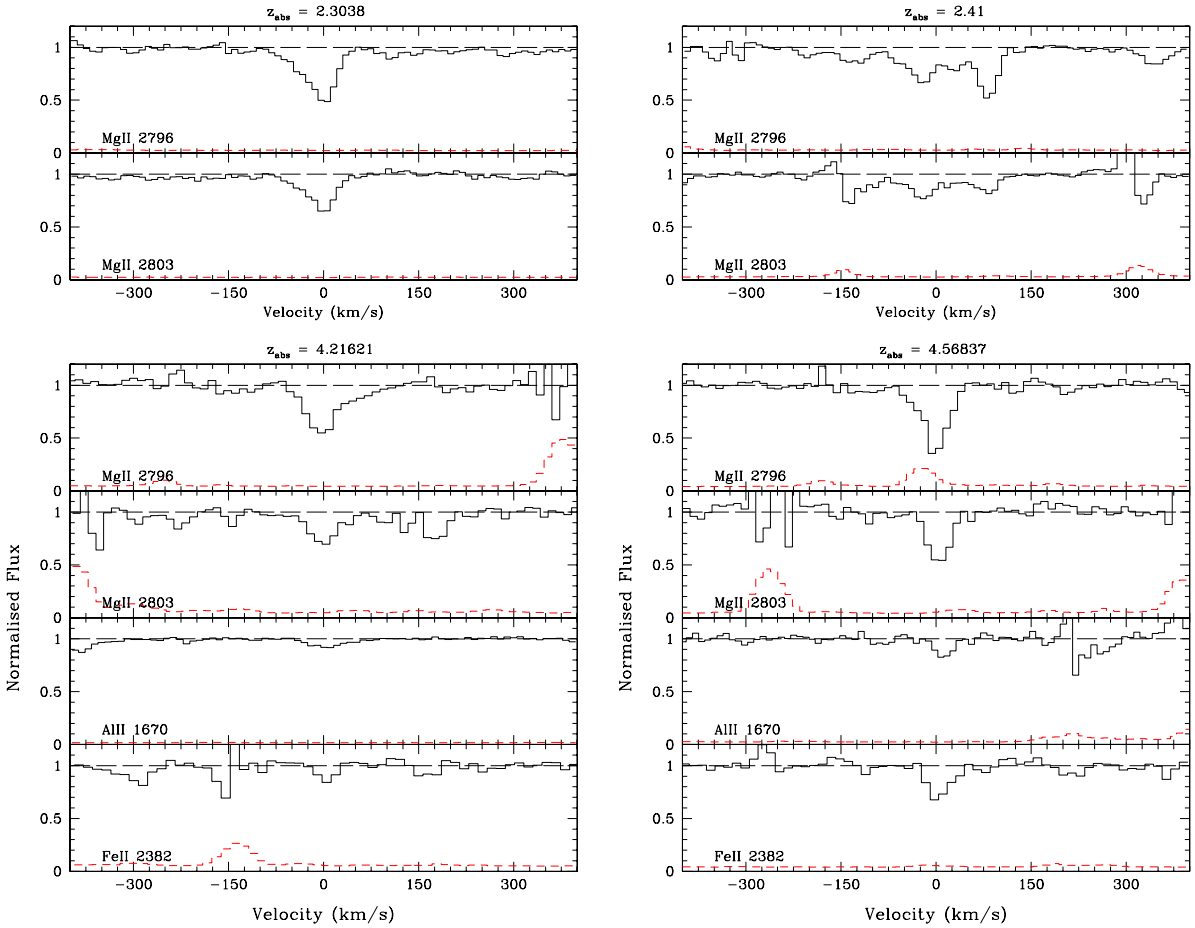

Figure B5. Mg II systems in the spectrum of ULAS J1319+0950.

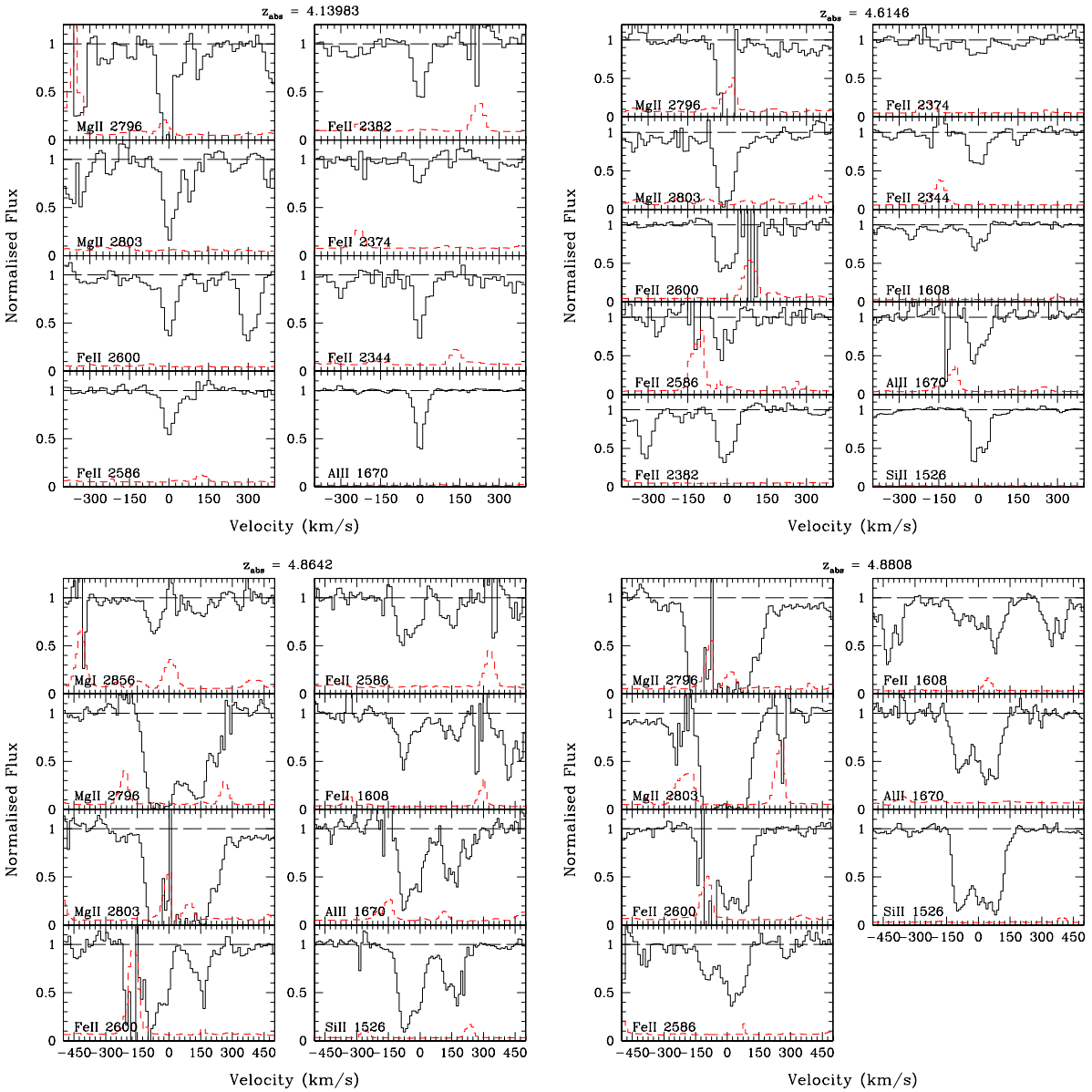

Figure B5 – *continued.*

B6 CFHQS J1509+1749

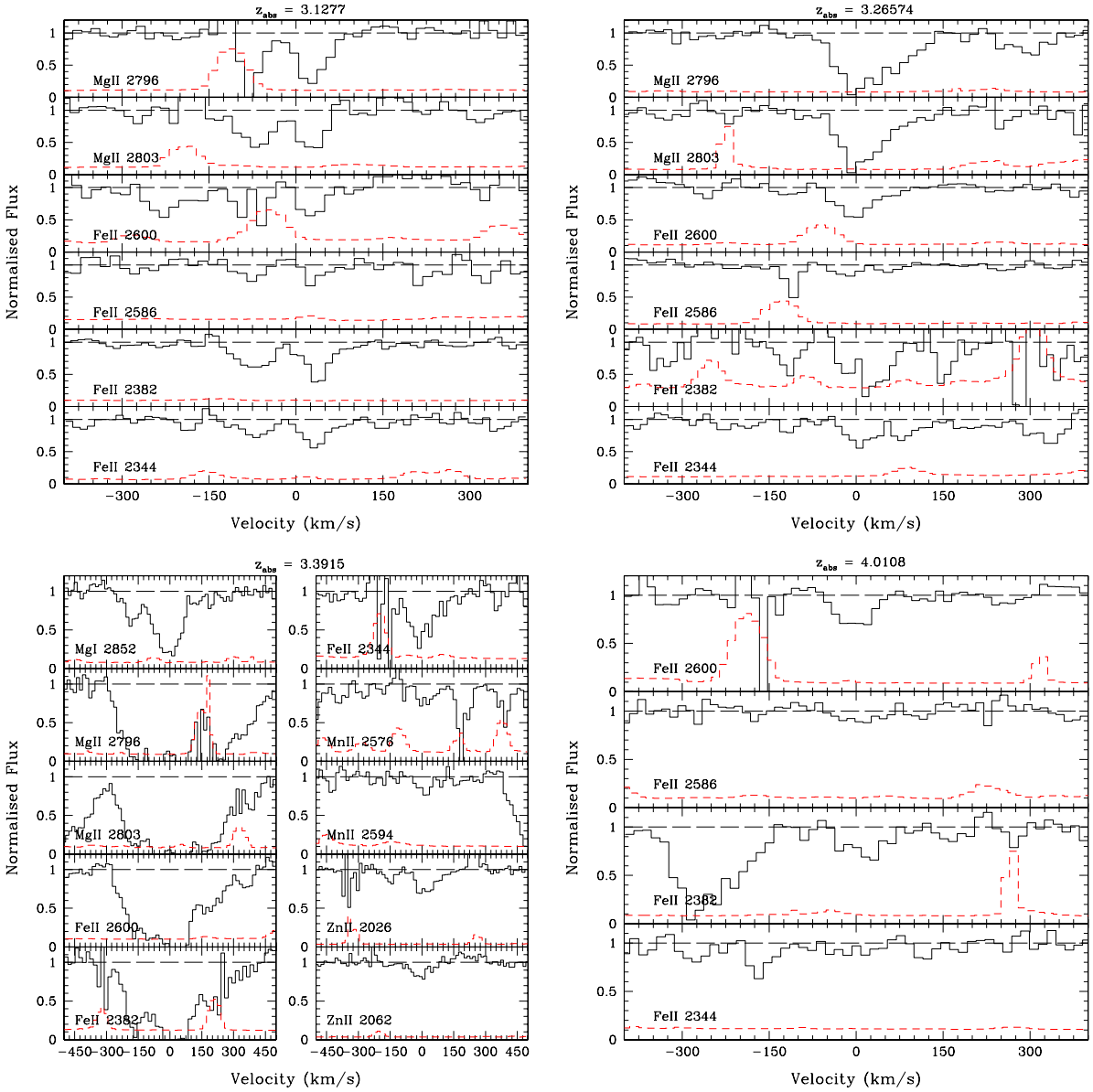

Figure B6. Mg II systems in the spectrum of CFHQS J1509−1749.

This paper has been typeset from a TEX/LATEX file prepared by the author.